Rationally Designed Potent and Selective CK1α Degraders Exert Antiproliferative Activity Against a Broad Range of Human Cancer Cell Lines

Zoran Rankovic (zoran.rankovic@stjude.org)
St. Jude Children's Research Hospital https://orcid.org/0000-0001-6866-4290
Gisele Nishiguchi
St. Jude Children's Research Hospital
Sherif Abdelhamed
St. Jude Children's Research Hospital
Sarah Young
St. Jude Children's Research Hospital
Elizabeth Caine
Promega
Lauren Mascibroda
St. Jude Children's Research Hospital
Jeffrey Kooijman
Oncolines
Sourav Das
St. Jude Children's Research Hospital
Darcie Miller
Saint Jude Childrens Hospital
Kevin McGowan
St. Jude Children's Research Hospital
Anand Mayasundari
Zhe Shi
St. Jude Children's Research Hospital
Juan Barajas
Ohio State University
Ryan Hiltenbrand
St. Jude Children's Research Hospital
Anup Aggarwal
St. Jude Children's Research Hospital
Yunchao Chang
St. Jude Children's Research Hospital

Vibhor Mishra
St. Jude Children's Research Hospital
Ravi Kalathur
St. Jude Children's Research Hospital https://orcid.org/0000-0002-4889-8003
Junmin Peng
St Jude Children's Research Hospital https://orcid.org/0000-0003-0472-7648
Shondra Pruett-Miller
St. Jude Children's Research Hospital https://orcid.org/0000-0002-3793-585X
Danette Daniels
Foghorn Therapeutics
Marjeta Urh
Promega https://orcid.org/0000-0003-2148-0341
Anang Shelat
St. Jude Children's Research Hospital https://orcid.org/0000-0002-6266-2910
Charles Mullighan
St. Jude Children's Research Hospital https://orcid.org/0000-0002-1871-1850
Kristin Riching
Promega Corporation https://orcid.org/0000-0003-4646-1067
Guido Zaman
Oncolines B.V.
Marcus Fischer
St. Jude Children's Research Hospital https://orcid.org/0000-0002-7179-2581
Jeffery Klco
St. Jude Children's Research Hospital https://orcid.org/0000-0003-2961-6960
Shilpa Narina
St. Jude Children's Research Hospital
Allister Loughran
St Jude children's research hospital https://orcid.org/0000-0002-6564-5526
Anthony High
St. Jude Children's Research Hospital

Article

Keywords:

Posted Date: May 12th, 2023

DOI: https://doi.org/10.21203/rs.3.rs-2883533/v1

Additional Declarations: Yes there is potential Competing Interest. Z.R. receives consulting fees from Revolution Medicines, Orum Therapeutics, Nyrada, and Vindur Therapeutics.

Version of Record: A version of this preprint was published at Nature Communications on January 16th, 2024. See the published version at https://doi.org/10.1038/s41467-024-44698-1.

Abstract

While the PROTAC approach to targeted protein degradation greatly benefits from rational design, the discovery of molecular glue degraders currently relies on screening strategies. Here, we describe screening of a library containing 3,630 cereblon binders against a panel of 9 patient-derived cancer cell lines. This led to the discovery of SJ7590, a potent degrader of CK1α, IKZF1 and IKZF3 proteins. Through a structure-guided optimization strategy we developed SJ3149, a uniquely potent and selective CK1α degrader. The crystal structure of the CK1α+CRBN+DDB1+SJ3149 quaternary complex provided a rationale for the improved degradation properties via direct contacts between SJ3149 and CK1α. In a panel of 115 human cancer cell lines SJ3149 displayed broad antiproliferative activity. This activity profile, which showed statistically significant correlation with MDM2 inhibitor Nutlin-3a, suggests potential for the development of treatments for hematological cancers, as well as solid tumors.

Introduction

The immunomodulatory imide drugs (IMiDs) thalidomide, lenalidomide and pomalidomide are the first drugs found to exert their pharmacological effect by inducing protein degradation. IMiDs bind cereblon (CRBN),[1] a substrate recognition domain of E3 ubiquitin ligase $CRL4^{CRBN}$. Altering its specificity results in the recruitment, ubiquitination, and subsequent degradation of proteins not normally targeted by the E3 ligase, termed neosubstrates. Two lymphoid transcription factors, IKZF1 and IKZF3, were first identified as IMiD neosubstrates, rationalizing the clinical efficacy of these drugs in multiple myeloma.[2] Subsequently, IMiDs were found to influence the abundance of numerous proteins, including SALL4,[3] ZBTB16,[4] p63,[5] ZFP91,[6] ZNF827, RAB28, and RNF166.[7,8]

Interestingly, lenalidomide is the only IMiD that was found to induce degradation of casein kinase 1A1 (CK1α), albeit with only a modest efficacy producing incomplete degradation at concentrations of up to 10 mM.[9] Nevertheless, the degradation of CK1a provides a mechanistic basis for lenalidomide's unique clinical efficacy in myelodysplastic syndrome (MDS) patients with deletion of chromosome 5q (del(5q)).[10] This is attributed to the haploinsufficiency of CK1a gene encoded at chromosome 5q32 (*CSNK1A1*), which heightens MDS sensitivity to the effects of lenalidomide-induced CK1α degradation. CK1α is a ubiquitously expressed cytosolic serine/threonine kinase involved in regulation of Wnt/b-catenin and p53 signaling.[11] The heterozygous loss of CK1a in del(5q) MDS stabilizes β-catenin, drives self-renewal and dominance of the del(5q) clone, whereas homozygous loss of CK1a, as occurs with lenalidomide-induced degradation of the haplodeficient CK1α, results in p53 induction and selective clonal arrest by virtue of synthetic lethality.[12] It is also interesting that CK1α silencing, using siRNA against *CSNK1A1*, potentiates apoptosis and growth arrest induced by lenalidomide in H929 cells,[13] suggesting that a more effective CK1α degrader may display even a greater potency.

Even though del(5q) is also a recurring abnormality in acute myeloid leukemia (AML), lenalidomide has shown limited clinical effect in AML.[14] This was proposed to be due to synthetic lethality that occurs only

in del(5q) MDS with haploinsufficient *CSNK1A1,* which is more likely to fail in AML since these leukemias with chromosome 5q abnormalities typically occur with other cytogenetic changes and often carry *TP53* mutations.[15] Nevertheless, CK1a has been found essential for AML cell survival in vitro and in vivo.[16] Pharmacologic inhibition of CK1α using D4476, a pan-CK1 inhibitor, or CK1α knockdown via lentivirus-mediated shRNA, suppressed proliferation and the clone formation by enhancing autophagic flux and apoptosis in both AML cell lines and patient blast cells.[17] In addition, AML patients have higher expression of *CSNK1A1* mRNA than healthy donors, and patients with high *CSNK1A1* have shorter overall survival.[17] Interestingly, a study in a panel of myeloid cancer cell lines showed that lenalidomide promoted the greatest degradation of CK1a in the most sensitive lines, such as HNT-34 and MDS-L, but did not degrade CK1a in the most insensitive line, MOLM-13.[18] In addition to MDS and AML,[19] CK1a was also found to promote survival of lymphoma cells,[20] as well as a variety of solid tumors such as in lung,[21] renal,[22] and colorectal[23] cancers, suggesting a potential broader clinical application of compounds that influence CK1a levels or activity. Recently, an elegant medicinal chemistry effort that produced selective CK1a, and dual CK1a/IKZF2 degraders were reported by Gray and Woo labs, respectively.[24,25]

This work employs our proprietary molecular glue library consisting of cereblon binders[26] to probe novel protein degradation mechanisms via small molecule degraders and neosubstrates. In this study, we report the results from screening this library against a panel of cancer cell lines and structure-guided optimization effort that led to the discovery of novel, highly potent and selective CK1α degraders (Fig 1).

Results

Phenotypic screening of a Molecular Glue Library against a panel of cancer cell lines identifies a hit with a unique cellular profile. We screened our molecular glue library (3,630 compounds) against a panel of 9 pediatric cancer cell lines to identify molecules displaying cell selective sensitivities. In addition to the four cell lines we previously described (MB002, MB004, HD-MB03 and MHHCALL-4), we included five additional AML cell lines (MOLM-13, TF-1, HEL, OCI-AML3 and AML193) to cover a broader range of genetic diversity and cancer vulnerabilities. The library screening was performed in high throughput (384-well plates) by incubating the cells with compounds for 72 hours and assessing cell viability via CellTiter-Glo (CTG) in a dose-response manner, as reported previously.[27]

As shown by the heatmap in Fig. 1a lenalidomide and pomalidomide were inactive (blue box), indicating that degradation of classical IMiD neosubstrates is not essential for the viability of these cell lines. CC-885[29] and our previously disclosed GSPT degrader (SJ6986)[27] were cytotoxic to all cell lines in the panel (yellow box, Fig. 1a), consistent with the previously observed anti-proliferative effect of degrading this essential protein. Clustering of hits by their activity profile across the cancer cell line panel identified one chemical series as cytotoxic and highly selective for MOLM-13 cells with IC_{50} < 1 μM (red box, Fig. 1a). Due to a distinct cell selectivity profile and high toxicity against MOLM-13 cells, we selected compound SJ7095 for further profiling (Fig. 1b).

Hit profiling identifies CK1α, IKZF1 and IKZF3 as main targets of SJ7095. Having identified SJ7095 as a compound with potent antiproliferative effect in MOLM-13 cells, we next examined whether the observed effect was CRBN-dependent. In ligand competition experiments, we treated MOLM-13 cells with SJ7095 in dose-response in the presence of high concentrations of lenalidomide (40 μM). Excess lenalidomide saturates the CRBN binding site making it inaccessible for other CRBN modulators, thereby abrogating the antiproliferative effects of SJ7095, as shown in Extended Data Fig. 1a. In an orthogonal approach, we tested SJ7095 in wild-type and CRBN-knockout MOLM-13 cells in a cell viability assay (Extended Data Fig. 1b). Our results unambiguously showed that the antiproliferative activity of SJ7095 was CRBN dependent.

We next carried out a tandem mass tag (TMT) quantitative proteomics experiment[30] to identify the neosubstrates whose degradation is induced by SJ7095. Upon treatment of MOLM-13 cells with SJ7095 over 4 hours at 5 μM concentration, significant degradation of only three proteins were observed, out of over 9,000 proteins identified: CK1α, IKZF1 and IKZF3 (Fig. 2a). This result was consistent at different concentrations and longer timepoint providing confidence in the overall selectivity profile (Extended Data Fig. 2). We confirmed the proteomics results by immunoblot analysis of CK1α in MOLM-13 cells following treatment with increasing concentrations of SJ7095 over 4 hours (Fig. 2b). Under these conditions compound SJ7095 induced dose-dependent reduction of CK1a protein levels with DC_{50} value of 15 nM. The degradation of CK1α was accompanied by a dose-dependent upregulation of p21, which was in agreement with our proteomics data and previously published studies in which CK1α inactivation resulted in p21-dependent cytotoxicity (Fig. 2b).[31]

The analysis of the publicly available dependency map data (DepMap) showed that MOLM-13 cells were highly dependent on CK1a while less sensitive to IKZF1 and IKZF3 CRISPR knock-out.[32] Similarly, MOLM-13 cells were the most dependent of all DepMap AML cell lines on siRNA-mediated silencing of CK1a. Importantly, potent IKZF1 degraders such as classical IMiDs (Fig. 1a), and more recently developed iberdomide (CC-220)[33] showed very little effect on the MOLM-13 cells' viability (Extended Data Fig.3a). Based on these observations we hypothesized that CK1α degradation was the main driver of the cell viability phenotype produced by compound SJ7095. To further validate this hypothesis, we performed CRISPR genomic editing of MOLM-13 using RNA guides against CK1a and measured the relative change of out-of-frame INDEL frequency at different time points. This provided further evidence of this cell line's dependency on CK1α (Extended Data Fig. 3b). We further confirmed these results by shRNA-targeted silencing of CK1a with a GFP reporter and measured the loss of GFP over time corresponding to the proliferative disadvantage of cells with CK1a knock-down (Extended Data Fig. 3c, d). Collectively, these data demonstrated a strong dependency of MOLM-13 cells on CK1a, which rationalized the observed viability effect of compound SJ7095 on this cell line.

Notably lenalidomide, the first and most characterized CK1a degrader, did not show appreciable cytotoxicity in MOLM-13 even at high concentrations (Fig.2c). Whereas treatment of MOLM-13 cells with 100 nM of SJ7095 over 4 hours induced a near complete degradation of CK1a, lenalidomide required a

1,000 times higher concentration (100 mM) and longer incubation time (24 h) to achieve a similar CK1a degradation effect (Fig. 2b). This suggests that the observed difference in cytotoxicity stems from lenalidomide's weaker CK1a degradation.

Structure-guided design leads to the discovery of selective CK1a degraders. While the potent and mixed CK1a and IKZF1/3 degradation profile displayed by SJ7095 has potential translational value, we were also interested in developing selective degraders that would be suitable for studying CK1a biology, as well as exploring potential therapeutic approaches for cancers where IKZF1/3 degradation is unnecessary or undesirable.[34,35,36]

To help with understanding the binding mode of SJ7095 and inform our optimization strategy, we performed molecular dynamics studies based on the previously reported crystal structure of lenalidomide in complex with CRBN/DDB1 and CK1a.[28] In the CRBN/DDB1-CK1a model the distal aromatic group in SJ7095 was aligned with the CRBN surface, and engaged with F150 in a loop (E147-I154) that was partly unresolved in the cereblon-lenalidomide-CK1a complex (PDB: 5FQD),[28] as shown in Fig. 1c. We postulated that this additional interaction with F150 resulted in increased cereblon stability and consequently greater stability of the ternary complex, ultimately leading to greater IKZF1 and CK1a degradation potency when compared to lenalidomide.[37] Importantly, besides the lenalidomide-like interaction between C7 of the solvent-exposed phthalimide ring and G40 of the β-hairpin loop (degron motif) in the N-lobe of CK1a, compound SJ7095 forms contacts only with CRBN. We hypothesized that molecules designed to establish additional stabilizing or destabilizing contacts with neosubstrates may display different degradation selectivity profiles. Specifically, we prioritized substitutions of C5 to engage residues in the β-hairpin loop of CK1a without disturbing the critical C7 interaction with G40 (Fig. 1c).

To evaluate this hypothesis, an array of C5-substituted amid analogues was synthesized and tested in MOLM-13 cells.[38] The most potent analogue was 3-methyl-benzamide SJ0040 (Fig. 1b), which inhibited MOLM-13 cell growth with IC_{50} of 14 nM, and reduced CK1a abundance with DC_{50} value of 11 nM and Dmax 88% (Fig 2b,c). Another round of optimization, which focused on replacing the benzamide group in SJ0040 with an array of heteroaromatic bioisosteres, led to the discovery of 3-amino-benzisoxazole SJ3149 (Fig. 1b). This compound proved to be the most potent CK1a degrader with DC_{50} of 3.7 nM and Dmax 95% (Fig. 2b). While IC_{50} of SJ3149 (13 nM) was similar to SJ0040 (14 nM), SJ3149 produced a more robust effect on the viability of MOLM-13 cells (Fig. 2c). As expected, neither of the two compounds affected CK1a levels in $CRBN^{-/-}$ MOLM-13 cells, confirming that their mechanism of action is CRBN-dependent (Extended Data Fig. 1c,d).Wild type and $CRBN^{-/-}$ MOLM-13 cells were also treated with 1 μM SJ7095, SJ0040, or SJ3149 for 24 and 72 hours to assess treatment-induced apoptosis by annexin staining (Extended Data Fig 4 and 5). Compared to control cells treated with DMSO, all three compounds led to increased cell death after 72 hours (Extended Data Fig 5a). SJ3149 caused the strongest effect with ~80% of cells dead or dying (Extended Data Fig 5b). Again, there was no effect on viability of the $CRBN^{-/-}$ cells (Extended Data Fig 5).

To better understand CK1a degradation properties, selectivity and mechanism of action, SJ0040 and SJ3149 were selected for evaluation against lenalidomide and the screening hit, SJ7095, in a panel of biochemical, biophysical and cellular assays.[38] To measure cellular protein levels, we used cell lines that have been engineered by CRISPR/Cas9 to express endogenous CK1α (HEK293 cells) or IKZF1 (Jurkat cells) with a HiBiT tag, which when coupled with LgBiT expression forms NanoBiT, a bioluminescent protein that can be used for kinetic studies of protein degradation.[39] Compounds were evaluated in a time-dependent and dose-response manner continuously over 24 hours period and degradation parameters were calculated as previously reported.[40] Cell viability was also monitored with CellTiter Glo 2.0 (Promega) at the completion of the experiment to ensure that loss of protein was not a consequence of a loss of cell viability. Data collected from these assays were used to generate an extensive multiparameter profile, which included neosubstrate specificity, DC_{50} (half-maximal degradation concentration at 4 hours post treatment), degradation rate constant, λ (computed from an exponential decay model fit of the kinetic degradation traces at 10 μM concentration), and Dmax (maximum protein degradation over the 24h timeframe at 10 μM concentration).

We first tested the compounds in the IKZF1 HiBiT (Jurkat cells) assay. As expected, lenalidomide and the original hit, SJ7095, induced significant IKZF1 protein degradation, with DC_{50} values of 0.033 mM and 0.069 mM at 4 hours, respectively. Importantly, neither of the two lead compounds, SJ0040 nor SJ3149, had an appreciable effect on the IKZF1 protein abundance (D_{max}<10%), validating our optimization strategy (Fig. 2d). Furthermore, in the CK1a HiBit assay our degraders demonstrated striking improvements in overall depth of CK1a degradation potency, and rate when compared to lenalidomide, and these improvements were further enhanced with each subsequent lead compound. In agreement with the immunoblotting results, maximum CK1α degradation induced by lenalidomide was only 42% in the CK1a HiBiT HEK293 cells at the highest concentration (10 mM). In contrast, SJ7095, SJ0040 and SJ3149 induced near-complete degradation of the CK1a protein, with DC_{50} values of 35 nM, 10 nM, and 6 nM at 4 hours, respectively (Fig. 2e). In addition, all three compounds exhibited a dramatic increase in degradation rate (Fig. 2f), with SJ3149 nearly 2-fold higher than SJ0040 and almost 10-fold over lenalidomide, likely driving the observed higher D_{max} and more potent degradation.

Interestingly, despite their superior degradation properties, the three compounds showed up to 8-fold lower affinity to CRBN than lenalidomide in our CRBN fluorescence polarization (FP) displacement assay (Fig. 2g). Indeed, we have previously noted that CRBN affinity is a poor predictor of degradation potency.[27] Experimental evidence reported over recent years suggest that ternary complex stability is a better predictor of degradation efficiency.[41] To determine whether CK1a degradation increased due to the compounds' improved ability to form ternary complex with CK1a, we transfected the CK1a HiBiT cells with a HaloTag-CRBN fusion and measured ternary complex formation by NanoBRET. Following 2 hours treatment, we observed dose-dependent increase in NanoBRET signal, indicating the formation of a ternary complex with CRBN induced by all our compounds (Fig. 2h). Notably, the ranking in ternary complex formation strongly mirrored the trends observed in degradation rate, D_{max} and potency, with the most robust complex formation induced by SJ3149.

Next, TMT-proteomics studies were performed to determine broader degradation selectivity profiles of our two lead compounds. This experiment showed that after a 4-hour incubation at 1 mM concentration both SJ0040 and SJ3419 significantly reduced abundance of only CK1a out of >9,000 proteins identified in MOLM-13 cells (Fig. 2i,j). As expected, increased protein levels of p53, p21 and b-catenin were detected in the treated cells.[31]

SJ3149 shows a broad antiproliferative profile. After establishing the potency and selectivity of our lead CK1a degraders, we investigated their effect on a panel of AML and ALL cell lines (Fig. 3a). While both compounds displayed cytotoxicity against all eight cell lines (CTG assay), SJ3149 proved to be most potent with IC_{50} values in a single digit nanomolar range, and even sub-nanomolar activity against UCSD-AML and PER117 cells (Fig 3a). Together these results demonstrate that SJ3149 is an exquisitely potent and selective CK1a degrader with a high activity across a range of acute leukemia (AL) cell lines.

To evaluate the compound's effect and potential therapeutic application across a diverse range of human cancers, we profiled SJ3149 in Oncolines® panel consisting of 115 human cancer cell lines, of which 86 were solid tumor and 29 hematologic cell lines, including MOLM-13. Effect on cell viability was monitored using ATPLite™ (Perkin Elmer), which measures intracellular ATP content as an indirect readout of cell number, like CellTiter Glo. IC_{50} and GI_{50} were determined after 72-hour treatment of cells with a duplicate 9-point dose range of compound. SJ3149 potently inhibited the viability of AML cell lines in the panel and cell lines derived from different hematologic neoplasms, such as B-cell and T-cell acute lymphoblastic leukemia (Fig. 3b).

Interestingly, SJ3149 also potently inhibited the viability of multiple cell lines derived from solid tumors, including breast, soft tissue, and tumors of the male and female reproductive system, with several cell lines being inhibited more potently than MOLM-13 (Fig. 3c, Supplementary Table 1). At the other end of the spectrum, multiple cell lines from diverse tumor tissue origins were insensitive (IC_{50} > 31.6 μM), demonstrating that SJ3149 is highly selective in cancer cell lines.

Since tissue-type alone could not explain the cell line responses to compound SJ3149, we investigated whether we could relate cell line sensitivity to genomic alterations in oncogenes or tumor suppressor genes. The mutation status of 38 frequently altered cancer genes was determined and cell lines were grouped according to either 'having' or 'not having' mutations, large deletions or amplifications, and gene translocations in these 38 genes (Supplementary Table 1)[42]. Analysis of variance (ANOVA) was performed to determine whether there were any significant associations between drug response and genetic features of the cell lines. Alterations in *TP53* were identified as the only significant drug response marker, where SJ3149 had, on average, 21-fold higher IC_{50} in *TP53*-altered cell lines compared to cell lines harboring wild-type *TP53* (Fig. 3d). This suggests that SJ3149 requires active wild type p53 signaling to exert its inhibitory effect in cell lines.

Our analysis of cell line sensitivity and the basal expression levels of 19,146 genes revealed expression of the p53 regulated gene SESN1 as a strong marker of cell line sensitivity to SJ3149 (Pearson's r = -0.44, p-

value = 4.0*10-6) (Fig. 3e).[43] Expression of *TP53* moderately, but significantly (r = -0.27; p-value = 0.01) correlated with sensitivity to SJ3149 (Fig. 3e). These results further support the finding that active p53 signaling is required for cell line response to SJ3149.

To further investigate the mechanism underlying the cell line selectivity of SJ3149, we compared its IC_{50} fingerprint in the viability assays with those of 120 other anti-cancer agents that have been profiled in 102 of the 115 cell lines. This revealed a significant correlation with nutlin-3a (r = 0.51; p-value = 1.0*10-7) (Fig. 3f). Nutlin-3a induces activation of p53 pathway and apoptosis by inhibiting p53 interaction with MDM2, an E3 ubiquitin-protein ligase that regulates p53 levels in cells.[44] Like SJ3149, nutlin-3a selectively targeted *TP53* wild-type cell lines (Fig. 3g). Although SJ3149 and nutlin-3a shared a relatively similar cell line targeting, SJ3149 inhibited responsive cell lines with low nanomolar or even sub-nanomolar potency, whereas nutlin-3a inhibited responsive cell lines with micromolar potency. Interestingly, SJ3149 showed the strongest correlation with *TP53* expression of all profiled agents (Fig. 3h).

Despite the significant overlap of the cell panel profiles of compound SJ3149 and nutlin-3a, the Pearson correlation of 0.51 indicated that there were also notable differences in the cellular context required for optimal cell killing activity of the two compounds. While having preference for *TP53* wild-type cell lines, SJ3149 also inhibited several *TP53*-altered cell lines that were insensitive to nutlin-3a (Fig. 3g). When we further investigated the different positions of *TP53* missense mutations, mutation of the lysine at position 132 to either a glutamine or arginine in BT-20 or KU812, respectively, conferred high sensitivity to SJ3149. SJ3149 had, on average, 2,500 times lower IC_{50} in these two cell lines, compared to cell lines harboring missense mutations on other positions in *TP53* (Fig. 3i). Given that lysine at position 132 is a reported ubiquitination site,[45] a selective CK1α degrader may therefore be more advantageous in targeting specific *TP53* mutant cancers compared to direct inhibition of the p53-MDM2 interaction.

To provide further insight into the cellular targeting of SJ3149 and differences from nutlin-3a, we correlated the IC_{50} profiles of both SJ3149 and nutlin-3a to cell line dependency profiles of more than 17,000 genes, based on large CRISPR screens.[46] As expected, the IC_{50} profile of nutlin-3a strongly correlated with dependency on MDM2 and MDM4, while *TP53* was strongly anti-correlated (Fig. 3j). Although SJ3149 was also significantly correlated with dependency on MDM2 and MDM4, these correlations were reduced compared to nutlin-3a (Figure 3k). In contrast to nutlin-3a, dependency on CRBN was significantly correlated with cell line response to SJ3149 (r = 0.38, p-value = 5.5*10-4), suggesting that direct targeting of CRBN may additionally contribute to the cellular inhibition profile of SJ3149.

The results of the cancer cell line profiling provide a rational for the application of selective CK1α degraders across a wide range of hematological and solid tumors. The cell line inhibition profile of SJ3149 strongly suggests preferential targeting of cell lines with wild-type *TP53* and certain *TP53* mutations, with marked potency and selectivity differences over nutlin-3a.

Structural basis of CK1α+CRBN+DDB1 ternary complex formation by SJ3149. To understand the molecular basis for the improved degradation potency of SJ3149 compared to lenalidomide, we pursued crystallography studies of the CK1α+CRBN+DDB1+SJ3149 quaternary complex (Fig. 4a). The resulting 3.45 Å crystal structure shows that the core scaffold which SJ3149 shares with lenalidomide is accommodated similarly in the same hydrophobic pocket of CRBN (Fig. 4b,c), except that residue E377 rotates to form a direct rather than a water-bridged interaction with SJ3149 (Fig. 4d). Interestingly, E377 was previously postulated to contribute to substrate specificity, as it preferentially interacts with lenalidomide over pomalidomide and thalidomide as targets for CK1α.[28] Unlike lenalidomide, which primes the CRBN interface for interaction with CK1α, SJ3149 forms several direct interactions with CK1α (Fig. 4b). SJ3149 engages with the CK1α N-terminal domain (NTD) via a hydrogen bond with K18 and several hydrophobic contacts with V20 and residues of the β-hairpin degron loop (from I35-G40) of CK1α (Fig. 4d), including G40 which is key for CRBN recruitment (Extended Data Fig. 6).[7,47] Mutation of G40 to an asparagine in the CK2α isoform prevents binding to CRBN, rendering CK2α undegraded, which exemplifies the importance for G40 in CRBN recruitment.[28] Upon extending into the solvent-exposed space, the novel benzisoxazol moiety of SJ3149 displaces a water molecule that is present in the lenalidomide-bound complex (PDB: 5FQD)[28] and forms a hydrogen bond with H353 of the CRBN C-terminal domain (CTD) (Fig. 4d). These anchoring hydrophobic and hydrogen bonding interactions at the CRBN-CK1α interface corroborate our modeling prediction that switching from C4 to C5 substitution provides a vector for a closer ternary complex.

It has been previously reported that upon ligand binding, the open apo state of CRBN rearranges into the closed state that is stabilized by a “sensor loop” (residues 351-354), which adopts a β-hairpin conformation upon closure and enables substrate binding and degradation.[37] When superimposed onto open (PDB: 8CVP) and closed (PDB: 8D81) CRBN, our structure confirms that CK1α is bound to the closed state of CRBN (Extended Data Fig. 7). A portion of the N-terminal Lon “belt” domain becomes ordered and wraps around the thalidomide binding domain (TBD) of CRBN for added stabilization (Extended Data Fig. 8). This stabilization of closed CRBN is thought to increase CK1α binding and enhance the stability of the ternary complex. With SJ3149 forming a hydrogen bond with H353 in the sensor loop (Fig. 4b,d) that is absent in the lenalidomide-bound complex, our structure hence proposes a molecular rationale for SJ3149’s increased degradation potency of CK1α compared to lenalidomide.

While our structure revealed several key new interactions the rest of the protein-protein interface appears largely unchanged compared to the lenalidomide complex, despite a subtle but notable rotation of CK1α (Extended Data Video). Finally, to establish the activation state of CK1α in the complex we superimposed our structure onto the active state of CK1α. Although no ATP was bound to its nucleotide binding site, CK1α’s DFG and HRD motifs flanking the disordered activation loop were in the same active state observed in the lenalidomide complex (Extended Data Fig. 9).[28,48]

To rationalize the degradation selectivity of SJ3149 for CK1a over IKZF1, we aligned our structure of SJ3149 with a previously reported structure of IKZF1 in complex with lenalidomide and CRBN+DDB1

(6H0F).[7] This model suggests that the change of the hydrophobic residue I35 in CK1a to the polar residue Q46 in the equivalent position in IKZF1 may destabilize the aromatic benzisoxazole moiety of SJ3149 and, at least in part, contribute to the compound's degradation selectivity over IKZF1 (Extended Data Fig. 10).

Discussion

Although CK1a is a potential target for hematological indications[49] there are no reported inhibitors nor degraders of this kinase with adequate potency and selectivity to enable pre-clinical validation studies. Lenalidomide is the only FDA approved drug known to induce, albeit weak, degradation of the CK1a protein. This may explain, at least in part, why lenalidomide shows meaningful clinical effect in MDS characterized by CK1a haploinsufficiency but lacks efficacy against AML in pre-clinical and clinical settings.[50] Herein, we report the discovery of potent and selective CK1a degraders with activity in a broad range of acute leukemia and solid tumor cell lines.

Screening of our library of CRBN-directed molecular glues against a panel of pediatric cancer cell lines, led to identification of SJ7095 with high cytotoxicity against MOLM-13 cells (IC_{50} = 71 nM), and potent CRBN-dependent degradation of CK1α, IKZF1 and IKZF3 proteins. This finding provided us with an initial confirmation that pharmacologically-induced CK1a degradation can phenocopy genetic knockdown experiments in MOLM-13 cells. Since our CRISPR and shRNA experiments showed that the loss of CK1a protein alone is sufficient to affect viability of MOLM-13 cells, we endeavored to develop selective CK1a degraders. Our structure-informed optimization focused on moving the substitution vector on the lenalidomide core of SJ7095 to establish direct interactions with the degron motif. Resulting SJ0040 and SJ3149 degraders displayed fast and potent CK1a degradation, proteome-wide selectivity, and improved antiproliferative effects in MOLM-13 cells. Both compounds were superior to lenalidomide with respect to the depth, kinetics, and potency of CK1a degradation. These observed improvements can be rationalized by CRBN-CK1a ternary complex formation induced in cells by the compounds. Indeed, the ranking in ternary complex formation directly reflected the trends observed in degradation potency, with the most robust complex formation induced by SJ3149 (Fig. 2h). The quaternary structure of CK1α+CRBN+DDB1+SJ3149 (Fig. 4) showed that, in contrast to lenalidomide, SJ3149 forms several direct interactions with CK1α, further validating our optimization hypothesis and rationalizing the improved ternary complex formation and ultimately CK1a degradation potency displayed by this compound.

SJ3149 also displayed superior activity against a panel of acute leukemia cell lines, with IC_{50} values in low nanomolar to sub-nanomolar range. Furthermore, in a larger panel of 115 human cancer cell lines SJ3149 potently decreased the viability of multiple solid tumor cell lines, including breast, soft tissue, and tumors of the male and female reproductive system, with several cell lines showing even greater sensitivity than MOLM-13 (Fig. 3). Interestingly, SJ3149 activity showed a strong correlation with wild-type *TP53* expression. An in depth analysis of IC_{50} fingerprints produced in this panel by SJ3149 and 120

other anti-cancer agents revealed a significant correlation with MDM2 inhibitor nutlin-3a (Fig. 3e).[44] This pharmacological similarity is not surprising, considering the role of CK1a in MDM2 activation and p53 pathway inhibition.[31] Interestingly, SJ3149 also inhibited several *TP53*-altered cell lines, such as BT-20 and KU812, suggesting that CK1a degraders may offer potential therapeutic opportunity for cancers that are insensitive to MDM2 inhibitors.

Overall, our study provides a rationale for the application of selective CK1α degraders across a wide range of hematologic and solid tumors. The cell line inhibition profile of SJ3149 strongly suggests preferential targeting of *TP53* wild-type cell lines, with marked potency and selectivity differences over Nutlin-3a. More generally, this study further supports the utility of a library of diverse CRBN binders in lead discovery, and ability to rationally optimize molecular glue potency and selectivity.

Declarations

Acknowledgements

We are grateful for the support of the American Lebanese Syrian Associated Charities (ALSAC) and St. Jude Children's Research Hospital, and we would like to thank the patients, their families, and the staff at our institution. This work was also supported in part by the Alex's Lemonade Stand Foundation Crazy 8 award. We thank A. Panchmatia for her help with the protein preparation that led to the structure, and A.S. Tanwar for initial expression test and purification. Data were collected at Southeast Regional Collaborative Access Team (SER-CAT) 22-ID (or 22-BM) beamline at the Advanced Photon Source, Argonne National Laboratory. SER-CAT is supported by its member institutions, and equipment grants (S10_RR25528, S10_RR028976 and S10_OD027000) from the National Institutes of Health. We also thank the Compound Management Center at the Department of Chemical Biology and Therapeutics for performing general QC and compound plate reformatting for screening.

Author Information

These authors contributed equally: Gisele Nishiguchi, Sherif Abdelhamed, Sarah Young

Authors and Affiliations

Department of Chemical Biology and Therapeutics, St. Jude Children's Research Hospital, Memphis, Tennessee 38105, USA.

Gisele Nishiguchi, Sarah Young, Sourav Das, Kevin McGowan, Anand Mayasundari,Zhe Shi, Anup Aggarwal, Anang Shelat, Marcus Fischer, Zoran Rankovic.

Department of Pathology, St. Jude Children's Research Hospital, 262 Danny Thomas Place, Memphis, TN 38105, USA.

Sherif Abdelhamed, Lauren G. Mascibroda, Juan M. Barajas, Ryan Hiltenbrand, Yunchao Chang, Vibhor Mishra, Charles Mullighan, Jeffery M. Klco

Promega Corporation, 5430 East Cheryl Drive, Madison, WI 53711, USA.

Elizabeth A. Caine, Danette L. Daniels, Marjeta Urh, Kristin M. Riching

Oncolines B.V., Kloosterstraat 9, 5349 AB Oss, The Netherlands

Jeffrey J. Kooijman, Guido J.R. Zaman

Department of Structural Biology, St. Jude Children's Research Hospital, 262 Danny Thomas Place, Memphis, TN 38105, USA.

Darcie Miller, Ravi Kalathur, Anthony A. High, Junmin Peng

Center for Advanced Genome Engineering, St. Jude Children's Research Hospital, Memphis, Tennessee 38105, USA.

Shondra M. Pruett-Miller, Shilpa Narina, Allister J. Loughran

Contributions

Z.R. conceived the study. J.M.K. directed biology studies. M.F. directed structural biology efforts. G.N. directed chemistry. S.Y. purified proteins; S.Y. and D.M. generated the crystal structure. S.A. and L.G.M. generated immunoblots, shRNA, CRISPR, and annexin data. S.D. and A.S. conducted in silico modeling. A.A.H. and J.P. performed proteomics studies. S.N., A.J.L., and S.M.P-M. generated CRBN$^{-/-}$ MOLM-13 cells. K.M. and Z.Z. performed chemistry synthesis. L.G.M, J.M.B, R.H., Y.C., V.M., A.A. and A.M. performed biochemical and cell-based assay screens. R.K. provided pellets for purification. E.A.C., D.L.D., M.U. and K.M.R. generated degradation kinetics data. J.J.K. and G.J.R.Z. performed Oncoline data analysis. The paper was written by G.N. and Z.R. with input from all authors.

Corresponding authors

Correspondence to: Marcus Fischer, Jeffery M. Klco, and Zoran Rankovic

Competing interests

The authors declare the following competing financial interest(s): Z.R. receives consulting fees from Revolution Medicines, Orum Therapeutics, Nyrada, and Vindur Therapeutics.

References

1. Ito, T.; Ando, H.; Suzuki, T.; Ogura, T.; Hotta, K.; Imamura, Y.; Yamaguchi, Y.; Handa, H. Identification of a Primary Target of Thalidomide Teratogenicity. *Science* **2010**, *327* (5971), 1345–1350.

https://doi.org/10.1126/science.1177319.

2. Krönke, J.; Udeshi, N. D.; Narla, A.; Grauman, P.; Hurst, S. N.; McConkey, M.; Svinkina, T.; Heckl, D.; Comer, E.; Li, X.; Ciarlo, C.; Hartman, E.; Munshi, N.; Schenone, M.; Schreiber, S. L.; Carr, S. A.; Ebert, B. L. Lenalidomide Causes Selective Degradation of IKZF1 and IKZF3 in Multiple Myeloma Cells. *Science* **2014**, *343* (6168), 301–305. https://doi.org/10.1126/science.1244851.
3. Matyskiela, M. E.; Couto, S.; Zheng, X.; Lu, G.; Hui, J.; Stamp, K.; Drew, C.; Ren, Y.; Wang, M.; Carpenter, A.; Lee, C.-W.; Clayton, T.; Fang, W.; Lu, C.-C.; Riley, M.; Abdubek, P.; Blease, K.; Hartke, J.; Kumar, G.; Vessey, R.; Rolfe, M.; Hamann, L. G.; Chamberlain, P. P. SALL4 Mediates Teratogenicity as a Thalidomide-Dependent Cereblon Substrate. *Nat. Chem. Biol.* **2018**, *14* (10), 981–987. https://doi.org/10.1038/s41589-018-0129-x.
4. Yamanaka, S.; Murai, H.; Saito, D.; Abe, G.; Tokunaga, E.; Iwasaki, T.; Takahashi, H.; Takeda, H.; Suzuki, T.; Shibata, N.; Tamura, K.; Sawasaki, T. Thalidomide and Its Metabolite 5-hydroxythalidomide Induce Teratogenicity via the Cereblon Neosubstrate PLZF. *EMBO J.* **2021**, *40* (4). https://doi.org/10.15252/embj.2020105375.
5. Asatsuma-Okumura, T.; Ando, H.; De Simone, M.; Yamamoto, J.; Sato, T.; Shimizu, N.; Asakawa, K.; Yamaguchi, Y.; Ito, T.; Guerrini, L.; Handa, H. P63 Is a Cereblon Substrate Involved in Thalidomide Teratogenicity. *Nat. Chem. Biol.* **2019**, *15* (11), 1077–1084. https://doi.org/10.1038/s41589-019-0366-7.
6. An, J.; Ponthier, C. M.; Sack, R.; Seebacher, J.; Stadler, M. B.; Donovan, K. A.; Fischer, E. S. PSILAC Mass Spectrometry Reveals ZFP91 as IMiD-Dependent Substrate of the CRL4CRBN Ubiquitin Ligase. *Nat. Commun.* **2017**, *8* (1), 15398. https://doi.org/10.1038/ncomms15398.
7. Sievers, Q. L.; Petzold, G.; Bunker, R. D.; Renneville, A.; Słabicki, M.; Liddicoat, B. J.; Abdulrahman, W.; Mikkelsen, T.; Ebert, B. L.; Thomä, N. H. Defining the Human C2H2 Zinc Finger Degrome Targeted by Thalidomide Analogs through CRBN. *Science* **2018**, *362* (6414), eaat0572. https://doi.org/10.1126/science.aat0572.
8. Donovan, K. A.; An, J.; Nowak, R. P.; Yuan, J. C.; Fink, E. C.; Berry, B. C.; Ebert, B. L.; Fischer, E. S. Thalidomide Promotes Degradation of SALL4, a Transcription Factor Implicated in Duane Radial Ray Syndrome. *eLife* **2018**, *7*, e38430. https://doi.org/10.7554/eLife.38430.
9. Krönke, J.; Fink, E. C.; Hollenbach, P. W.; MacBeth, K. J.; Hurst, S. N.; Udeshi, N. D.; Chamberlain, P. P.; Mani, D. R.; Man, H. W.; Gandhi, A. K.; Svinkina, T.; Schneider, R. K.; McConkey, M.; Järås, M.; Griffiths, E.; Wetzler, M.; Bullinger, L.; Cathers, B. E.; Carr, S. A.; Chopra, R.; Ebert, B. L. Lenalidomide Induces Ubiquitination and Degradation of CK1α in Del(5q) MDS. *Nature* **2015**, *523* (7559), 183–188. https://doi.org/10.1038/nature14610.
10. List, A.; Dewald, G.; Bennett, J.; Giagounidis, A.; Raza, A.; Feldman, E.; Powell, B.; Greenberg, P.; Thomas, D.; Stone, R.; Reeder, C.; Wride, K.; Patin, J.; Schmidt, M.; Zeldis, J.; Knight, R. Lenalidomide in the Myelodysplastic Syndrome with Chromosome 5q Deletion. *N. Engl. J. Med.* **2006**, *355* (14), 1456–1465. https://doi.org/10.1056/NEJMoa061292.

11. Jiang, S.; Zhang, M.; Sun, J.; Yang, X. Casein Kinase 1α: Biological Mechanisms and Theranostic Potential. *Cell Commun. Signal.* **2018**, *16* (1), 23. https://doi.org/10.1186/s12964-018-0236-z.
12. Schneider, R. K.; Ademà, V.; Heckl, D.; Järås, M.; Mallo, M.; Lord, A. M.; Chu, L. P.; McConkey, M. E.; Kramann, R.; Mullally, A.; Bejar, R.; Solé, F.; Ebert, B. L. Role of Casein Kinase 1A1 in the Biology and Targeted Therapy of Del(5q) MDS. *Cancer Cell* **2014**, *26* (4), 509–520. https://doi.org/10.1016/j.ccr.2014.08.001.
13. Manni, S.; Carrino, M.; Manzoni, M.; Gianesin, K.; Nunes, S. C.; Costacurta, M.; Tubi, L. Q.; Macaccaro, P.; Taiana, E.; Cabrelle, A.; Barilà, G.; Martines, A.; Zambello, R.; Bonaldi, L.; Trentin, L.; Neri, A.; Semenzato, G.; Piazza, F. Inactivation of CK1α in Multiple Myeloma Empowers Drug Cytotoxicity by Affecting AKT and β-Catenin Survival Signaling Pathways. *Oncotarget* **2017**, *8* (9), 14604–14619. https://doi.org/10.18632/oncotarget.14654.
14. Sekeres, M. A.; Gundacker, H.; Lancet, J.; Advani, A.; Petersdorf, S.; Liesveld, J.; Mulford, D.; Norwood, T.; Willman, C. L.; Appelbaum, F. R.; List, A. F. A Phase 2 Study of Lenalidomide Monotherapy in Patients with Deletion 5q Acute Myeloid Leukemia: Southwest Oncology Group Study S0605. *Blood* **2011**, *118* (3), 523–528. https://doi.org/10.1182/blood-2011-02-337303.
15. Ebert, B. L. Molecular Dissection of the 5q Deletion in Myelodysplastic Syndrome. *Semin. Oncol.* **2011**, *38* (5), 621–626. https://doi.org/10.1053/j.seminoncol.2011.04.010.
16. Järås, M.; Miller, P. G.; Chu, L. P.; Puram, R. V.; Fink, E. C.; Schneider, R. K.; Al-Shahrour, F.; Peña, P.; Breyfogle, L. J.; Hartwell, K. A.; McConkey, M. E.; Cowley, G. S.; Root, D. E.; Kharas, M. G.; Mullally, A.; Ebert, B. L. Csnk1a1 Inhibition Has P53-Dependent Therapeutic Efficacy in Acute Myeloid Leukemia. *J. Exp. Med.* **2014**, *211* (4), 605–612. https://doi.org/10.1084/jem.20131033.
17. Xu, W.; Huang, Z.; Gan, Y.; Chen, R.; Huang, Y.; Xue, B.; Jiang, S.; Yu, Z.; Yu, K.; Zhang, S. Casein Kinase 1α Inhibits P53 Downstream of MDM2-mediated Autophagy and Apoptosis in Acute Myeloid Leukemia. *Oncol. Rep.* **2020**. https://doi.org/10.3892/or.2020.7760.
18. Hollenbach, P.; Lu, L.; Gandhi, A. K.; Chopra, R.; MacBeth, K. J. Lenalidomide Promotes Degradation of Casein Kinase 1a (CK1a) through Cereblon: Implications for the Efficacy of Lenalidomide in MDS and AML. *Blood* **2014**, *124* (21), 3606–3606. https://doi.org/10.1182/blood.V124.21.3606.3606.
19. Janovská, P.; Normant, E.; Miskin, H.; Bryja, V. Targeting Casein Kinase 1 (CK1) in Hematological Cancers. *Int. J. Mol. Sci.* **2020**, *21* (23), 9026. https://doi.org/10.3390/ijms21239026.
20. Bidère, N.; Ngo, V. N.; Lee, J.; Collins, C.; Zheng, L.; Wan, F.; Davis, R. E.; Lenz, G.; Anderson, D. E.; Arnoult, D.; Vazquez, A.; Sakai, K.; Zhang, J.; Meng, Z.; Veenstra, T. D.; Staudt, L. M.; Lenardo, M. J. Casein Kinase 1α Governs Antigen-Receptor-Induced NF-KB Activation and Human Lymphoma Cell Survival. *Nature* **2009**, *458* (7234), 92–96. https://doi.org/10.1038/nature07613.
21. Bowman, B. M.; Sebolt, K. A.; Hoff, B. A.; Boes, J. L.; Daniels, D. L.; Heist, K. A.; Galbán, C. J.; Patel, R. M.; Zhang, J.; Beer, D. G.; Ross, B. D.; Rehemtulla, A.; Galbán, S. Phosphorylation of FADD by the Kinase CK1α Promotes KRAS ^{G12D} -Induced Lung Cancer. *Sci. Signal.* **2015**, *8* (361). https://doi.org/10.1126/scisignal.2005607.

22. Mai, H.; Xu, X.; Mei, G.; Hong, T.; Huang, J.; Wang, T.; Yan, Z.; Li, Y.; Liang, Y.; Li, L.; Jin, S.; You, W.; Ma, Y.; Chen, L.; Ye, Q. The Interplay between HPIP and Casein Kinase 1α Promotes Renal Cell Carcinoma Growth and Metastasis via Activation of MTOR Pathway. *Oncogenesis* **2016**, *5* (10), e260–e260. https://doi.org/10.1038/oncsis.2016.44.
23. Richter, J.; Kretz, A.-L.; Lemke, J.; Fauler, M.; Werner, J.-U.; Paschke, S.; Leithäuser, F.; Henne-Bruns, D.; Hillenbrand, A.; Knippschild, U. CK1α Overexpression Correlates with Poor Survival in Colorectal Cancer. *BMC Cancer* **2018**, *18* (1), 140. https://doi.org/10.1186/s12885-018-4019-0.
24. Teng, M.; Lu, W.; Donovan, K. A.; Sun, J.; Krupnick, N. M.; Nowak, R. P.; Li, Y.-D.; Sperling, A. S.; Zhang, T.; Ebert, B. L.; Fischer, E. S.; Gray, N. S. Development of PDE6D and CK1α Degraders through Chemical Derivatization of FPFT-2216. *J. Med. Chem.* **2022**, *65* (1), 747–756. https://doi.org/10.1021/acs.jmedchem.1c01832.
25. Park, S. M.; Miyamoto, D.; Han, G.; Chan, M.; Curnutt, N.; Tran, N.; Velleca, A.; Kim, J. H.; Schurer, A.; Chang, K.; Woo, C. M.; Kharas, M. G. Dual IKZF2 and CK1α Degrader Targets Acute Myeloid Leukemia Cells. *Blood* **2022**, *140* (Supplement 1), 675–676. https://doi.org/10.1182/blood-2022-167678.
26. Hollenbach, P.; Lu, L.; Gandhi, A. K.; Chopra, R.; MacBeth, K. J. Lenalidomide Promotes Degradation of Casein Kinase 1a (CK1a) through Cereblon: Implications for the Efficacy of Lenalidomide in MDS and AML. *Blood* **2014**, *124* (21), 3606. https://doi.org/10.1182/blood.V124.21.3606.3606.
27. Nishiguchi, G.; Keramatnia, F.; Min, J.; Chang, Y.; Jonchere, B.; Das, S.; Actis, M.; Price, J.; Chepyala, D.; Young, B.; McGowan, K.; Slavish, P. J.; Mayasundari, A.; Jarusiewicz, J. A.; Yang, L.; Li, Y.; Fu, X.; Garrett, S. H.; Papizan, J. B.; Kodali, K.; Peng, J.; Pruett Miller, S. M.; Roussel, M. F.; Mullighan, C.; Fischer, M.; Rankovic, Z. Identification of Potent, Selective, and Orally Bioavailable Small-Molecule GSPT1/2 Degraders from a Focused Library of Cereblon Modulators. *J. Med. Chem.* **2021**, acs.jmedchem.0c01313. https://doi.org/10.1021/acs.jmedchem.0c01313.
28. Petzold, G.; Fischer, E. S.; Thomä, N. H. Structural Basis of Lenalidomide-Induced CK1α Degradation by the CRL4CRBN Ubiquitin Ligase. *Nature* **2016**, *532* (7597), 127–130. https://doi.org/10.1038/nature16979.
29. Hansen, J. D.; Condroski, K.; Correa, M.; Muller, G.; Man, H.-W.; Ruchelman, A.; Zhang, W.; Vocanson, F.; Crea, T.; Liu, W.; Lu, G.; Baculi, F.; LeBrun, L.; Mahmoudi, A.; Carmel, G.; Hickman, M.; Lu, C.-C. Protein Degradation via CRL4 ^{CRBN} Ubiquitin Ligase: Discovery and Structure–Activity Relationships of Novel Glutarimide Analogs That Promote Degradation of Aiolos and/or GSPT1. *J. Med. Chem.* **2018**, *61* (2), 492–503. https://doi.org/10.1021/acs.jmedchem.6b01911.
30. Bai, B.; Tan, H.; Pagala, V. R.; High, A. A.; Ichhaporia, V. P.; Hendershot, L.; Peng, J. Deep Profiling of Proteome and Phosphoproteome by Isobaric Labeling, Extensive Liquid Chromatography, and Mass Spectrometry. In *Methods in Enzymology*; Elsevier, 2017; Vol. 585, pp 377–395. https://doi.org/10.1016/bs.mie.2016.10.007.
31. Huart, A.-S.; MacLaine, N. J.; Meek, D. W.; Hupp, T. R. CK1α Plays a Central Role in Mediating MDM2 Control of P53 and E2F-1 Protein Stability. *J. Biol. Chem.* **2009**, *284* (47), 32384–32394. https://doi.org/10.1074/jbc.M109.052647.

32. Portal[1].
33. Lonial, S.; Popat, R.; Hulin, C.; Jagannath, S.; Oriol, A.; Richardson, P. G.; Facon, T.; Weisel, K.; Larsen, J. T.; Minnema, M. C.; Abdallah, A.-O.; Badros, A. Z.; Knop, S.; Stadtmauer, E. A.; Cheng, Y.; Amatangelo, M.; Chen, M.; Nguyen, T. V.; Amin, A.; Peluso, T.; van de Donk, N. W. C. J. Iberdomide plus Dexamethasone in Heavily Pretreated Late-Line Relapsed or Refractory Multiple Myeloma (CC-220-MM-001): A Multicentre, Multicohort, Open-Label, Phase 1/2 Trial. *Lancet Haematol.* **2022**, *9* (11), e822–e832. https://doi.org/10.1016/S2352-3026(22)00290-3.
34. John, L. B.; Ward, A. C. The Ikaros Gene Family: Transcriptional Regulators of Hematopoiesis and Immunity. *Mol. Immunol.* **2011**, *48* (9–10), 1272–1278. https://doi.org/10.1016/j.molimm.2011.03.006.
35. Olsson, L.; Johansson, B. Ikaros and Leukaemia. *Br. J. Haematol.* **2015**, *169* (4), 479–491. https://doi.org/10.1111/bjh.13342.
36. Marke, R.; van Leeuwen, F. N.; Scheijen, B. The Many Faces of IKZF1 in B-Cell Precursor Acute Lymphoblastic Leukemia. *Haematologica* **2018**, *103* (4), 565–574. https://doi.org/10.3324/haematol.2017.185603.
37. Watson, E. R.; Novick, S.; Matyskiela, M. E.; Chamberlain, P. P.; H. de la Peña, A.; Zhu, J.; Tran, E.; Griffin, P. R.; Wertz, I. E.; Lander, G. C. Molecular Glue CELMoD Compounds Are Regulators of Cereblon Conformation. *Science* **2022**, *378* (6619), 549–553. https://doi.org/10.1126/science.add7574.
38. Kozicka, Z.; Thomä, N. H. Haven't Got a Glue: Protein Surface Variation for the Design of Molecular Glue Degraders. *Cell Chem. Biol.* **2021**, *28* (7), 1032–1047. https://doi.org/10.1016/j.chembiol.2021.04.009.
39. Riching, K. M.; Mahan, S.; Corona, C. R.; McDougall, M.; Vasta, J. D.; Robers, M. B.; Urh, M.; Daniels, D. L. Quantitative Live-Cell Kinetic Degradation and Mechanistic Profiling of PROTAC Mode of Action. *ACS Chem. Biol.* **2018**, *13* (9), 2758–2770. https://doi.org/10.1021/acschembio.8b00692.
40. Riching, K. M.; Mahan, S.; Corona, C. R.; McDougall, M.; Vasta, J. D.; Robers, M. B.; Urh, M.; Daniels, D. L. Quantitative Live-Cell Kinetic Degradation and Mechanistic Profiling of PROTAC Mode of Action. *ACS Chem. Biol.* **2018**, *13* (9), 2758–2770. https://doi.org/10.1021/acschembio.8b00692.
41. Hughes, S. J.; Ciulli, A. Molecular Recognition of Ternary Complexes: A New Dimension in the Structure-Guided Design of Chemical Degraders. *Essays Biochem.* **2017**, *61* (5), 505–516. https://doi.org/10.1042/EBC20170041.
42. Zaman, G. J. R.; de Roos, J. A. D. M.; Libouban, M. A. A.; Prinsen, M. B. W.; de Man, J.; Buijsman, R. C.; Uitdehaag, J. C. M. TTK Inhibitors as a Targeted Therapy for *CTNNB1* (**β** -Catenin) Mutant Cancers. *Mol. Cancer Ther.* **2017**, *16* (11), 2609–2617. https://doi.org/10.1158/1535-7163.MCT-17-0342.
43. Velasco-Miguel, S.; Buckbinder, L.; Jean, P.; Gelbert, L.; Talbott, R.; Laidlaw, J.; Seizinger, B.; Kley, N. PA26, a Novel Target of the P53 Tumor Suppressor and Member of the GADD Family of DNA Damage and Growth Arrest Inducible Genes. *Oncogene* **1999**, *18* (1), 127–137. https://doi.org/10.1038/sj.onc.1202274.

44. Vassilev, L. T.; Vu, B. T.; Graves, B.; Carvajal, D.; Podlaski, F.; Filipovic, Z.; Kong, N.; Kammlott, U.; Lukacs, C.; Klein, C.; Fotouhi, N.; Liu, E. A. In Vivo Activation of the P53 Pathway by Small-Molecule Antagonists of MDM2. *Science* **2004**, *303* (5659), 844–848. https://doi.org/10.1126/science.1092472.

45. Nie, L.; Sasaki, M.; Maki, C. G. Regulation of P53 Nuclear Export through Sequential Changes in Conformation and Ubiquitination. *J. Biol. Chem.* **2007**, *282* (19), 14616–14625. https://doi.org/10.1074/jbc.M610515200.

46. Pacini, C.; Dempster, J. M.; Boyle, I.; Gonçalves, E.; Najgebauer, H.; Karakoc, E.; van der Meer, D.; Barthorpe, A.; Lightfoot, H.; Jaaks, P.; McFarland, J. M.; Garnett, M. J.; Tsherniak, A.; Iorio, F. Integrated Cross-Study Datasets of Genetic Dependencies in Cancer. *Nat. Commun.* **2021**, *12* (1), 1661. https://doi.org/10.1038/s41467-021-21898-7.

47. Matyskiela, M. E.; Lu, G.; Ito, T.; Pagarigan, B.; Lu, C.-C.; Miller, K.; Fang, W.; Wang, N.-Y.; Nguyen, D.; Houston, J.; Carmel, G.; Tran, T.; Riley, M.; Nosaka, L.; Lander, G. C.; Gaidarova, S.; Xu, S.; Ruchelman, A. L.; Handa, H.; Carmichael, J.; Daniel, T. O.; Cathers, B. E.; Lopez-Girona, A.; Chamberlain, P. P. A Novel Cereblon Modulator Recruits GSPT1 to the CRL4CRBN Ubiquitin Ligase. *Nature* **2016**, *535* (7611), 252–257. https://doi.org/10.1038/nature18611.

48. Kornev, A. P.; Haste, N. M.; Taylor, S. S.; Ten Eyck, L. F. Surface Comparison of Active and Inactive Protein Kinases Identifies a Conserved Activation Mechanism. *Proc. Natl. Acad. Sci.* **2006**, *103* (47), 17783–17788. https://doi.org/10.1073/pnas.0607656103.

49. Janovská, P.; Normant, E.; Miskin, H.; Bryja, V. Targeting Casein Kinase 1 (CK1) in Hematological Cancers. *Int. J. Mol. Sci.* **2020**, *21* (23), 9026. https://doi.org/10.3390/ijms21239026.

50. Löwenberg, B.; Pabst, T.; Maertens, J.; Gradowska, P.; Biemond, B. J.; Spertini, O.; Vellenga, E.; Griskevicius, L.; Tick, L. W.; Jongen-Lavrencic, M.; van Marwijk Kooy, M.; Vekemans, M.-C.; van der Velden, W. J. F. M.; Beverloo, B.; Michaux, L.; Graux, C.; Deeren, D.; de Weerdt, O.; van Esser, J. W. J.; Bargetzi, M.; Klein, S. K.; Gadisseur, A.; Westerweel, P. E.; Veelken, H.; Gregor, M.; Silzle, T.; van Lammeren-Venema, D.; Moors, I.; Breems, D. A.; Hoogendoorn, M.; Legdeur, M.-C. J. C.; Fischer, T.; Kuball, J.; Cornelissen, J.; Porkka, K.; Juliusson, G.; Meyer, P.; Höglund, M.; Gjertsen, B. T.; Janssen, J. J. W. M.; Huls, G.; Passweg, J.; Cloos, J.; Valk, P. J. M.; van Elssen, C. H. M. J.; Manz, M. G.; Floisand, Y.; Ossenkoppele, G. J. Addition of Lenalidomide to Intensive Treatment in Younger and Middle-Aged Adults with Newly Diagnosed AML: The HOVON-SAKK-132 Trial. *Blood Adv.* **2021**, *5* (4), 1110–1121. https://doi.org/10.1182/bloodadvances.2020003855.

51. Milde, T.; Lodrini, M.; Savelyeva, L.; Korshunov, A.; Kool, M.; Brueckner, L. M.; Antunes, A. S. L. M.; Oehme, I.; Pekrun, A.; Pfister, S. M.; Kulozik, A. E.; Witt, O.; Deubzer, H. E. HD-MB03 Is a Novel Group 3 Medulloblastoma Model Demonstrating Sensitivity to Histone Deacetylase Inhibitor Treatment. *J. Neurooncol.* **2012**, *110* (3), 335–348. https://doi.org/10.1007/s11060-012-0978-1.

52. Shadrick, W. R.; Slavish, P. J.; Chai, S. C.; Waddell, B.; Connelly, M.; Low, J. A.; Tallant, C.; Young, B. M.; Bharatham, N.; Knapp, S.; Boyd, V. A.; Morfouace, M.; Roussel, M. F.; Chen, T.; Lee, R. E.; Kiplin Guy, R.; Shelat, A. A.; Potter, P. M. Exploiting a Water Network to Achieve Enthalpy-Driven, Bromodomain-

Selective BET Inhibitors. *Bioorg. Med. Chem.* **2018**, *26* (1), 25–36. https://doi.org/10.1016/j.bmc.2017.10.042.

53. Bandopadhayay, P.; Bergthold, G.; Nguyen, B.; Schubert, S.; Gholamin, S.; Tang, Y.; Bolin, S.; Schumacher, S. E.; Zeid, R.; Masoud, S.; Yu, F.; Vue, N.; Gibson, W. J.; Paolella, B. R.; Mitra, S. S.; Cheshier, S. H.; Qi, J.; Liu, K.-W.; Wechsler-Reya, R.; Weiss, W. A.; Swartling, F. J.; Kieran, M. W.; Bradner, J. E.; Beroukhim, R.; Cho, Y.-J. BET Bromodomain Inhibition of MYC-Amplified Medulloblastoma. *Clin. Cancer Res.* **2014**, *20* (4), 912–925. https://doi.org/10.1158/1078-0432.CCR-13-2281.
54. Petzold, G.; Fischer, E. S.; Thomä, N. H. Structural Basis of Lenalidomide-Induced CK1α Degradation by the CRL4(CRBN) Ubiquitin Ligase. *Nature* **2016**, *532* (7597), 127–130. https://doi.org/10.1038/nature16979.
55. Madhavi Sastry, G.; Adzhigirey, M.; Day, T.; Annabhimoju, R.; Sherman, W. Protein and Ligand Preparation: Parameters, Protocols, and Influence on Virtual Screening Enrichments. *J. Comput. Aided Mol. Des.* **2013**, *27* (3), 221–234. https://doi.org/10.1007/s10822-013-9644-8.
56. Friesner, R. A.; Murphy, R. B.; Repasky, M. P.; Frye, L. L.; Greenwood, J. R.; Halgren, T. A.; Sanschagrin, P. C.; Mainz, D. T. Extra Precision Glide: Docking and Scoring Incorporating a Model of Hydrophobic Enclosure for Protein–Ligand Complexes. *J. Med. Chem.* **2006**, *49* (21), 6177–6196. https://doi.org/10.1021/jm051256o.
57. Bai, B.; Tan, H.; Pagala, V. R.; High, A. A.; Ichhaporia, V. P.; Hendershot, L.; Peng, J. Deep Profiling of Proteome and Phosphoproteome by Isobaric Labeling, Extensive Liquid Chromatography, and Mass Spectrometry. In *Methods in Enzymology*; Elsevier, 2017; Vol. 585, pp 377–395. https://doi.org/10.1016/bs.mie.2016.10.007.
58. Sentmanat, M. F.; Peters, S. T.; Florian, C. P.; Connelly, J. P.; Pruett-Miller, S. M. A Survey of Validation Strategies for CRISPR-Cas9 Editing. *Sci. Rep.* **2018**, *8* (1), 888. https://doi.org/10.1038/s41598-018-19441-8.
59. Connelly, J. P.; Pruett-Miller, S. M. CRIS.Py: A Versatile and High-Throughput Analysis Program for CRISPR-Based Genome Editing. *Sci. Rep.* **2019**, *9* (1), 4194. https://doi.org/10.1038/s41598-019-40896-w.
60. Matyskiela, M. E.; Zhang, W.; Man, H.-W.; Muller, G.; Khambatta, G.; Baculi, F.; Hickman, M.; LeBrun, L.; Pagarigan, B.; Carmel, G.; Lu, C.-C.; Lu, G.; Riley, M.; Satoh, Y.; Schafer, P.; Daniel, T. O.; Carmichael, J.; Cathers, B. E.; Chamberlain, P. P. A Cereblon Modulator (CC-220) with Improved Degradation of Ikaros and Aiolos. *J. Med. Chem.* **2018**, *61* (2), 535–542. https://doi.org/10.1021/acs.jmedchem.6b01921.
61. Kooijman, J. J.; van Riel, W. E.; Dylus, J.; Prinsen, M. B. W.; Grobben, Y.; de Bitter, T. J. J.; van Doornmalen, A. M.; Melis, J. J. T. M.; Uitdehaag, J. C. M.; Narumi, Y.; Kawase, Y.; de Roos, J. A. D. M.; Willemsen-Seegers, N.; Zaman, G. J. R. Comparative Kinase and Cancer Cell Panel Profiling of Kinase Inhibitors Approved for Clinical Use from 2018 to 2020. *Front. Oncol.* **2022**, *12*, 953013. https://doi.org/10.3389/fonc.2022.953013.
62. Iorio, F.; Knijnenburg, T. A.; Vis, D. J.; Bignell, G. R.; Menden, M. P.; Schubert, M.; Aben, N.; Gonçalves, E.; Barthorpe, S.; Lightfoot, H.; Cokelaer, T.; Greninger, P.; van Dyk, E.; Chang, H.; de Silva, H.; Heyn, H.;

Deng, X.; Egan, R. K.; Liu, Q.; Mironenko, T.; Mitropoulos, X.; Richardson, L.; Wang, J.; Zhang, T.; Moran, S.; Sayols, S.; Soleimani, M.; Tamborero, D.; Lopez-Bigas, N.; Ross-Macdonald, P.; Esteller, M.; Gray, N. S.; Haber, D. A.; Stratton, M. R.; Benes, C. H.; Wessels, L. F. A.; Saez-Rodriguez, J.; McDermott, U.; Garnett, M. J. A Landscape of Pharmacogenomic Interactions in Cancer. *Cell* **2016**, *166* (3), 740–754. https://doi.org/10.1016/j.cell.2016.06.017.

63. Zaman, G. J. R.; de Roos, J. A. D. M.; Libouban, M. A. A.; Prinsen, M. B. W.; de Man, J.; Buijsman, R. C.; Uitdehaag, J. C. M. TTK Inhibitors as a Targeted Therapy for *CTNNB1* (**β** -Catenin) Mutant Cancers. *Mol. Cancer Ther.* **2017**, *16* (11), 2609–2617. https://doi.org/10.1158/1535-7163.MCT-17-0342.
64. Smeby, J.; Sveen, A.; Eilertsen, I. A.; Danielsen, S. A.; Hoff, A. M.; Eide, P. W.; Johannessen, B.; Hektoen, M.; Skotheim, R. I.; Guren, M. G.; Nesbakken, A.; Lothe, R. A. Transcriptional and Functional Consequences of *TP53* Splice Mutations in Colorectal Cancer. *Oncogenesis* **2019**, *8* (6), 35. https://doi.org/10.1038/s41389-019-0141-3.
65. Abdulrahman, W.; Uhring, M.; Kolb-Cheynel, I.; Garnier, J.-M.; Moras, D.; Rochel, N.; Busso, D.; Poterszman, A. A Set of Baculovirus Transfer Vectors for Screening of Affinity Tags and Parallel Expression Strategies. *Anal. Biochem.* **2009**, *385* (2), 383–385. https://doi.org/10.1016/j.ab.2008.10.044.
66. Kabsch, W. *XDS*. *Acta Crystallogr. D Biol. Crystallogr.* **2010**, *66* (2), 125–132. https://doi.org/10.1107/S0907444909047337.
67. McCoy, A. J.; Grosse-Kunstleve, R. W.; Adams, P. D.; Winn, M. D.; Storoni, L. C.; Read, R. J. *Phaser* Crystallographic Software. *J. Appl. Crystallogr.* **2007**, *40* (4), 658–674. https://doi.org/10.1107/S0021889807021206.
68. Emsley, P.; Lohkamp, B.; Scott, W. G.; Cowtan, K. Features and Development of *Coot*. *Acta Crystallogr. D Biol. Crystallogr.* **2010**, *66* (4), 486–501. https://doi.org/10.1107/S0907444910007493.
69. Liebschner, D.; Afonine, P. V.; Baker, M. L.; Bunkóczi, G.; Chen, V. B.; Croll, T. I.; Hintze, B.; Hung, L.-W.; Jain, S.; McCoy, A. J.; Moriarty, N. W.; Oeffner, R. D.; Poon, B. K.; Prisant, M. G.; Read, R. J.; Richardson, J. S.; Richardson, D. C.; Sammito, M. D.; Sobolev, O. V.; Stockwell, D. H.; Terwilliger, T. C.; Urzhumtsev, A. G.; Videau, L. L.; Williams, C. J.; Adams, P. D. Macromolecular Structure Determination Using X-Rays, Neutrons and Electrons: Recent Developments in *Phenix*. *Acta Crystallogr. Sect. Struct. Biol.* **2019**, *75* (10), 861–877. https://doi.org/10.1107/S2059798319011471.

Methods

Molecular Glue Library Screening. The primary screen was performed in 384-well format using the Cell-Titer Glo (CTG) luminescent cell viability assay (Promega) as previously described.[27] 3,630 compounds from the St. Jude proprietary molecular glue library were screened against 9 human cancer cell lines (HD-MB03, MB004, MB002, MHH-CALL4, MOLM-13, TF-1, HEL, OCI-AML3, AML193). Each cell line was cultured in the complete medium recommended by the vendor and seeded in Corning 8804 BC white 384-well assay plates at densities of 1000, 1000, 1500, 7500, 1250, 156, 625, 1250, 1250 cells per well for HD-MB03, MB004, MB002, MHH-CALL4, MOLM-13, TF-1, HEL, OCI-AML, AML193, respectively. After

overnight incubation at 37 °C in a humidified 5% CO_2 incubator, cells were treated with compounds in dose-response format using a Pintool on a Biomek FX^P Laboratory Automation Workstation (Beckman Coulter). After 72 h of incubation, cell proliferation was assessed using a Cell Titer-Glo (CTG) luminescent cell viability assay (Promega) according to the manufacturer's instruction. Luminescence signal was measured using an EnVision plate reader (PerkinElmer).

Cell lines and cell culture. HD-MB03 cell line was obtained from Drs. Milde, Witt and Deubzer.[51] HD-MB03 and MB004 cells were grown in neurobasal medium supplemented with glutamine, streptomycin, penicillin, B27, EGF, bFGF and heparin as previously described.[52] MB002 and MB004 cells were obtained from Dr Yoon-Jae Cho.[53] MB002 cells were cultured in 80% neurobasal medium supplemented with glutamine, streptomycin, penicillin, B27 and 20% conditioned media from previous passages; EGF, bFGF and heparin were also added to the medium. MHH-CALL4 cells were obtained from German Collection of Microorganisms and Cell Cultures GmbH (DSMZ, Germany) and were cultured in RPMI1640 medium supplemented with 10% FBS (Hyclone), Penicillin/Streptomycin (100 units/mL) and Glutamine (100 µM). Cell identity was confirmed by STR profiling using PowerPlex® Fusion System (Promega). MHH-CALL4, NALM-16, MHH-CALL-2 cells were obtained from German Collection of Microorganisms and Cell Cultures GmbH (DSMZ, Germany). PER-117 cells were obtained from Telethon Kids Institute (Perth, Australia). The cells were cultured in RPMI1640 medium supplemented with 10% FBS (Hyclone), Penicillin/Streptomycin (100 units/mL) and Glutamine (100 µM) except for MHH-CALL-2 cells where 20% FBS were used. MOLM-13 cells were obtained from DSMZ (ACC 554) and cultured in RPMI-1640 media (Gibco) supplemented with 20% FBS (R&D Systems) and 100 U/ml penicillin-streptomycin (Gibco). HNT-34 cells were purchased from DSMZ (ACC 600) and cultured in RPMI-1640 media supplemented with 20% FBS and 100 U/ml penicillin-streptomycin. Kasumi-3 cells were purchased from ATCC (CRL-2725) and cultured in RPMI-1640 media supplemented with 20% FBS and 100 U/ml penicillin-streptomycin. UCSD-AML1 cells were purchased from DSMZ (ACC 691) and cultured in RPMI-1640 media supplemented with 20% FBS, 100 U/ml penicillin-streptomycin, and 10 ng/ml human GM-CSF (PeproTech). TF-1 cells were purchased from DSMZ (ACC 334) and cultured in RPMI-1640 media supplemented with 20% FBS, 100 U/ml penicillin-streptomycin, and 5 ng/ml human GM-CSF. OCI-AML3 cells were purchased from DSMZ (ACC 690) and cultured in Alpha-MEM media (Invitrogen) supplemented with 20% FBS and 100 U/ml penicillin-streptomycin. HEL cells were obtained from Dr. Charles Mullighan and cultured in RPMI-1640 media supplemented with 10% FBS and 100 U/ml penicillin-streptomycin. AML193 cells were purchased from DSMZ (ACC 549) cultured in IMDM supplemented with 5% FBS, 100 U/ml penicillin-streptomycin, Insulin-Transferrin-Selenium (ITS-G, Gibco), and 5 ng/ml human GM-CSF. Cell identity was confirmed by STR profiling using PowerPlex® Fusion System (Promega).

Modeling SJ7095 in CK1α. Molecular modeling work was done using the Schrodinger Maestro molecular modeling package (Schrödinger Release 2019-4: LigPrep, Schrödinger, LLC, New York, NY, 2019). A lenalidomide bound complex structure was obtained from the PDB (PDB code: 5FQD).[54] Only chains B (CRBN) and C (CK1α) were retained and the resulting structure was prepared using the Protein Preparation Wizard[55] such that the missing loop Gln148-Glu153 in cereblon was reconstructed. The tool

allowed hydrogen-bond optimization and restrained minimization of the complex (converge heavy atoms to RMSD 0.3 A). This structure was relaxed using a molecular dynamics simulation at 300K and 1.01325 bar pressure using a water-box. SPC waters and an orthorhombic boundary box with 15A buffer was chosen and the system was neutralized by adding Cl- ions. OPLS3e forcefield was used to simulate the system in GPU-accelerated Desmond (Schrödinger Release 2019-4: Desmond Molecular Dynamics System, D. E. Shaw Research, New York, NY, 2019. Maestro-Desmond Interoperability Tools, Schrödinger, New York, NY, 2019.). An NPT ensemble was used with timestep of 2 fs and Coulombic short range cutoff radius was set at 9Å. Upon completion of the simulation, the water molecules were removed and SJ7095 was docked in the place of the Lenalidomide molecule using Schrodinger Glide Extra Precision (XP) method[56] and the docked complex was further simulated for 500 ns using the parameters defined earlier, to obtain the SJ7095-CRBN-CK1α complex.

Proteomics in MOLM-13. Each compound was tested in 3 wells of 2 million MOLM-13 cells each. Cells were treated in tissue culture-treated 6-well plates in 3 ml total media volume and incubated at 37°C for 4 hours. Cells were then collected and washed with DPBS. Washed cells were centrifuged at 400 RCF for 5 minutes at 4°C, supernatant was removed, and pellets were snap frozen in liquid nitrogen and stored at -80°C until sample submission.

Protein Digestion and Peptide Isobaric Labeling by TMT Reagents. The experiment was performed with a previously optimized protocol[57] with slight modification. Cell pellets were lysed in lysis buffer (50 mM HEPES, pH 8.5, 8 M urea and 0.5% sodium deoxycholate). To profile whole proteome, the protein lysates (approximately 100 µg of protein per sample were proteolyzed with LysC (Wako) at an enzyme-to-substrate ratio of 1:100 (w/w) for 2 h at 21 ^{o}C. Following this the samples were diluted to a final 2 M Urea concentration, and further digested with trypsin (Promega) at an enzyme-to-substrate ratio of 1:50 (w/w) for at least 3 h. The peptides were reduced by adding 1 mM DTT for 30 min at 21^{o}C followed by alkylation with 10 mM iodoacetamide for 30 min in the dark. The unreacted IAA was quenched with 30 mM DTT for 30 min. Finally, the digestion was stopped by adding trifluoroacetic acid (TFA) to 1%, desalted using C18 cartridges (Harvard Apparatus) and dried by speedvac. The purified peptides were resuspended in 50 mM HEPES (pH 8.5), labeled with TMT reagents (Thermo Scientific). The differentially labeled samples were pooled equally, desalted and dried for the subsequent peptide fractionation. Peptide Analysis by two-dimensional liquid chromatography-Tandem Mass Spectrometry (LC/LC-MS/MS) and MS Data analysis are described in the Supplementary Material.

Western blotting. Frozen pellets of ~1 million cells were lysed in 150 ul of SDS lysis buffer (60 mM Tris/HCl pH 7, 10% glycerol, 2% SDS, 5% beta mercaptoethanol, 0.02% bromophenol blue, 0.5% protease and phosphatase inhibitor cocktail (Sigma Aldrich)). When cells were resuspended, samples were heated for 3 minutes at 99°C then put on ice. Samples were then fragmented by sonication for 10 0.5-second pulses (550 Sonic Dismembrator, Fisher Scientific) and heated again at 99°C for 2 minutes. 16 µl of each sample was added to the wells of a 4-20% polyacrylamide gel (Bio-Rad). A mixture of 2 µl of Precision Plus Protein Unstained Standards and 2 µl of Precision Plus Protein All Blue Standards (Bio-Rad) was used for size marker. After electrophoresis, gels were transferred to nitrocellulose membrane using the

Bio-Rad Trans-Blot Turbo system on the mixed molecular weight setting. Membranes were blocked for 1 hour in Li-Cor Intercept Blocking Buffer then probed overnight at 4°C with primary antibody in Li-Cor Intercept Antibody Diluent. The following morning, membranes were washed 3 times for 5 minutes with TBS + Tween-20, probed with fluorescent secondary antibodies (goat anti-rabbit IRDye 800CW and goat anti-mouse IRDye 680RD, Li-Cor) for 1 hour at room temperature in the dark, and washed again 3 times. Blots were imaged with the Li-Cor Odyssey CLx and analyzed using Image Studio Version 5.2.

Antibodies. Primary antibodies used:
rabbit anti-CK1α, ab206652, Abcam
rabbit anti-p21, 2947S, Cell Signaling Technology
mouse anti-beta actin, 3700S, Cell Signaling Technology

shRNA. MOLM-13 cells were transduced with shRNA lentiviral particles from non-targeting control (NTC) and 3 CK1 shRNAs (CSNK1a1-a, CSNK1a1-b, CSNK1a1-c). Cells were then sorted after 3 days of culture for GFP+ cells. After sorting, 5.0E+03 cells were from each condition were harvested for immunoblot assay. An equal number of cells (5.0E+06) from each condition were then plated in triplicates. Cells were then grown for 13 days and change in GFP+ cells was assessed by flow cytometry at days 0, 3, 6, 10, and 13 pos-sort.

shRNA plasmid information

Name:	Company	Catalog #	Target Sequence
NTC shRNA	GeneCopoeia	CSHCTR001-1-LVRU6GP	GGTTGTGGACAACCATTTACT
CK1 -shRNA #1	GeneCopoeia	HSH059457-LVRU6GP-a	GGTTGTGGACAACCATTTACT
CK1 -shRNA #2	GeneCopoeia	HSH059457-LVRU6GP-b	GCAGAATTTGCGATGTACTTA
CK1 -shRNA #3	GeneCopoeia	HSH059457-LVRU6GP-c	CCCTGAACCATCAATATGACT

MOLM-13 CRBN Knock-out. $CRBN^{-/-}$ MOLM-13 cells were created using CRISPR-Cas9 technology. Briefly, 1 million MOLM-13 cells were transiently transfected with precomplexed ribonuclear proteins (RNPs) consisting of 400pmol of chemically modified sgRNA (Synthego), 135pmol of *Sp*Cas9 protein (St. Jude Protein Production Core), and 500ng of pMaxGFP (Lonza) via nucleofection (Lonza, 4D-Nucleofector™ X-unit) using solution SF and program EO100 in a 100ul cuvette according to the manufacturer's recommended protocol. Transfected cells (GFP+) were single-cell sorted by flow cytometry (St. Jude Flow Cytometry and Cell Sorting Shared Resource) into 96-well tissue culture treated plates five days post nucleofection. Cells were clonally expanded and screened for the desired targeted modification (out-of-frame indels) via targeted deep sequencing using gene specific primers with partial Illumina adapter overhangs as previously described.[58] Genotyping of clones was performed using CRIS.py.[59] Knockout clones were identified as clones containing only out-of-frame indels. PowerPlex® Fusion System

(Promega) was used to confirm final clone identification (Hartwell Center for Biotechnology at St. Jude). All clones tested negative for mycoplasma by the MycoAlert^{TM}Plus Mycoplasma Detection Kit (Lonza). CRBN knockout confirmed by immunoblot (Supplementary Material).

Dependency assay. Dependency assay for CSNK1A1 was performed by nucleofecting precomplexed RNP (150pmol CSNK1A1 gRNA with 50pmol Cas9 protein) in 20ul P3 solution with program EO100. Two different gRNAs were tested separately (CAGE1215.CSNK1A1.g1 and CAGE1215.CSNK1A1.g7). Following nucleofection, cells were cultured at 37C, 5% CO2, and gDNA samples were taken at days 3, 7, 14, and 21 post transfection. Indel profiles were analyzed using CRIS.py. The sequences of the sgRNA spacers and associated genotyping primers are show in Table 1.

Table 1. The sequences of the CSNK1A1 sgRNA spacers and associated genotyping primers

Name	Sequence (5' to 3')
SM148.CRBN.g3 spacer	UGUAUGUGAUGUCGGCAGAC
CAGE1215.CSNK1A1.g1 spacer	UUCUAGUCGCCGAGAUGACA
CAGE1215.CSNK1A1.g7 spacer	UUUACCUUUAGCCCUUGCCA
Forward indexing primer (5'-3')	AATGATACGGCGACCACCGAGATCTACAC(6bp index)ACACTCTTTCCCTACACGACGCTCTTC
Reverse indexing primer (5'-3')	CAAGCAGAAGACGGCATACGAGAT(10bp index)GTGACTGGAGTTCAGACGTGTGCTC
SM148.hCRBN.DS.F2	ctacacgacgctcttccgatctGCAGAGAGTGAGGAAGAAGATGA
SM148.hCRBN.DS.R2	cagacgtgtgctcttccgatctGCCCATGTCCTCATCCACAA
CAGE1215.CSNK1A1.F	ctacacgacgctcttccgatctCACCAAATAGTGTTCCCTCCTCA
CAGE1215.CSNK1A1.R	cagacgtgtgctcttccgatctTGGGTACCAGCTTACTGTCTCT

CRBN Fluorescence Polarization Assay. In this competitive fluorescent polarization assay Cy5 conjugated lenalidomide analog (Cy5-O-Len)[60] was used as the fluorescent probe. The assay cocktail was prepared by combining 6XHis-CRBN-DDB1 protein (200 nM) and Cy5-O-Len probe (30 nM) in 20 mM HEPES pH 7, 150 mM NaCl, 0.005% Tween-20 assay buffer. Compounds were transferred to a Corning 3821 black 384-well assay plate from a dose-response plate using a Labcyte Echo 650 Acoustic Liquid Handler (Beckman Coulter, USA). Then 20 mL of the assay cocktail was dispensed to wells of the assay plate with a Multidrop Combi Reagent Dispenser (Thermo Scientific, USA). The plates were incubated in the dark for 1 hour at room temperature and then read on an Envision plate reader (PerkinElmer, USA). IC_{50} values were determined using a proprietary software RISE (Robust Investigation of Screening Experiments),

developed in house on the Pipeline Pilot platform (Biovia, v. 17.2.0). Data represent the mean of three independent determinations.

HiBiT-tagged Cell Culture. CSNK1A1-HiBiT HEK293 LgBiT stable CRISPR edited clonal cells (Promega, Cat. #CS3023104) and HiBiT-GSPT1 HEK293 LgBiT stable CRISPR edited clonal cells (Promega, Cat. #CS3023106) and HEK293 cells (ATCC, Cat. #CRL-1573) were maintained in DMEM (Gibco, Cat. #11995065) supplemented with 10% FBS (VWR, Cat.# 89510-194). IKZF1-HiBiT Jurkat LgBiT stable cells (Promega, Cat. #CS3023170) were maintained in RPMI-1640 (Gibco, Cat. #11875093) supplemented with 10% FBS.

Degradation and Cell Viability Assays. White 96-well assay plates (Corning, Cat. # 3017) were seeded with 30,000 cells/well in growth media for CSNK1A1-HiBiT HEK293 LgBiT stable and HiBiT-GSPT1 HEK293 LgBiT stable and incubated overnight at 37°C and 5% CO_2. After the overnight incubation, the medium on the CSNK1A1-HiBiT HEK293 LgBiT stable and HiBiT-GSPT1 HEK293 LgBiT stable cells was aspirated off and replaced with CO_2 independent medium (Gibco, Cat. #18045088) supplemented with 10% FBS and 1x Endurazine (Promega, Cat. #N2571) substrate. IKZF1-HiBiT Jurkat LgBiT stable cells were seeded at 60,000 cells/well in 50% growth media/50% CO_2 independent medium supplemented with 10% FBS and 1x Endurazine substrate. Luminescence was allowed to equilibrate for all plates for 2.5 hours.

A dose response curve was generated by performing 3-fold dilutions of each compound including a DMSO only control in growth media. For live cell kinetic degradation assays, diluted compounds were added to CSNK1A1 and GSPT1 plates and placed in a GloMax Discover (Promega, Cat. #GM3000) preheated to 37°C or added to IKZF1 plates and placed in a CLARIOstar Plus (BMG LABTECH) preheated to 37°C. Luminescence was read every 5-15 minutes for 24 hours. At the end of all 24-hour cycles, CellTiter Glo 2.0 (Promega, Cat. #G9242) was added to the plates, incubated for at least 10 minutes and luminescence was read using the GloMax Discover.

Relative protein level was determined based on normalization to the DMSO control and reported at Fractional RLUs. Degradation rate, degradation maximums, and DC50 at 4 hours was calculated from Fractional RLUs as previously described[39].

Live Cell Ternary Complex NanoBRET Assays. CSNK1A1-HiBiT HEK293 LgBiT stable and HiBiT-GSPT1 HEK293 LgBiT stable cells were transfected with a HaloTag-CRBN vector (Promega, Cat. #N269A) using Fugene HD (Promega, Cat. #E2311). HEK293 cells were transfected with a NanoLuc-IKZF1 and HaloTag-CRBN vector at a 1:100 ratio using Fugene HD and incubated overnight at 37°C with 5% CO_2. Following overnight incubation, cells were replated in OptiMEM I Reduced Serum Medium, no phenol red (Gibco, Cat. #11058021) supplemented with 4% FBS, and HaloTag 618 ligand (Promega, Cat. #G9801). Plates were incubated overnight at 37°C with 5% CO_2. On day 3, a dose response curve was generated by performing 3-fold dilutions of each compound including a DMSO only control in OptiMEM I Reduced Serum Medium, no phenol red supplemented with 4% FBS. Cells were treated with MG132 (Selleckchem, Cat. #S2619) for

30 minutes before being treated with the dilution series of compounds. Plates were incubated for 2 hours at 37°C with 5% CO_2. After 2 hours, plates were read using NanoBRET Nano-Glo substate (Promega #N1573) on a GloMax Discover following manufacturer's instructions. No ligand controls were subtracted from each sample and normalized to the no compound DMSO control to obtain Fractional BRET values. EC50 values were calculated for each compound curve.

Annexin-V staining for apoptosis. Wild type and CRBN-/- MOLM-13 cells were grown in 12-well plates (TPP) with 500,000 cells per well in 2 ml total media volume. Cells were treated with 1 µl/ml DMSO or 1 µM compound in triplicate, and incubated for 24 or 72 hours at 37°C. To prepare samples, this buffer was used: 10 mM HEPES, 0.14 M NaCl, 2.5 mM $CaCl_2$ pH 7.4, 2% v/v FBS in UltraPure water (Invitrogen). After incubation, samples were collected in 5-ml tubes for flow cytometry (Falcon). Single-stain controls consisted of approximately 150 µl of multiple samples combined. Wells were washed with 1 ml of buffer that was added to the corresponding sample tube. Cells were centrifuged at 500 RCF for 5 minutes at 4°C to form a pellet. Supernatant was decanted and cells were washed again with 3 ml of buffer, then centrifuged. After decanting supernatant, 3 µl of APC-conjugated anti-Annexin-V antibody (BioLegend) was added to each tube in the residual buffer left behind. Samples were mixed by vortex and incubated at room temperature in the dark for 20 minutes. Samples were then washed and centrifuged a final time, decanting the supernatant and blotting the tubes to removed residual buffer. 50 µl of buffer with DAPI was added to all appropriate samples and mixed, then analyzed.

Oncolines® cancer cell lines. Cell lines were purchased from the American Type Culture Collection (ATCC) (Manassas, VA, USA) or German Collection of Microorganisms and Cell Cultures (DSMZ) (Braunschweig, Germany). All experiments were carried out within ten passages of the original vials. Authenticity of the cell lines was confirmed by short tandem repeat analysis at the respective provider.

Oncolines® SJ3149 cell viability assays. Cell viability assays were performed as previously described.[61] In brief, cells were seeded in a 384-well plate at an optimized density. The starting cell number was determined after 24 hours incubation by adding ATPlite 1Step (PerkinElmer, Groningen, the Netherlands) to each well and recording luminescence on an Envision multimode reader (PerkinElmer, Waltham, MA). After addition of a duplicate 9-point dilution series of SJ3149, cells were incubated for another 72 hours, followed by cell counting using ATPlite 1Step. The dilution series ranged from 3.2 nM to 31,600 nM or was diluted 100-fold for the most sensitive cell lines to ideally capture the complete dose-response curve. Percentage viability was determined at each compound concentration by relating the observed signal to a vehicle-treated control, that is, medium containing 0.4% (v/v) DMSO. Compound IC_{50} values were calculated by fitting a 4-parameter logistic curve to the percentage viability values using IDBS XLfit5 (IDBS, Guildford, United Kingdom). The IC_{50} was limited to the maximum tested compound concentration when the IC_{50} exceeded the maximum tested concentration. All dose-response curves were visually inspected and submitted to an F-test, followed by invalidation of curves with $F > 1.5$. $^{10}\log(IC_{50}[\text{nmol/L}])$ values were used for bioinformatics analyses, unless otherwise indicated.

Oncolines® cell line genomics. Genomic status of 37 frequently altered cancer genes was retrieved from the COSMIC Cell Lines Project (v80) database[62,63]. Mutations, large deletions or amplifications, and gene translocations were considered relevant genomic alterations. Only non-synonymous alterations which directly altered the coding sequence were retained for further analysis. Furthermore, mutations were filtered for occurrence in primary patient samples. Mutation status of *TP53* was retrieved from the DepMap database (version 22Q4). Considering the diverse spectrum of protein function-altering *TP53* mutations, all non-synonymous mutations were retained for this gene (Extended Data Table).[64] All 38 genes were altered in at least three cell lines. For each gene, the difference in average $^{10}\log IC_{50}$ between altered and wild-type cell lines was determined. Significance of the IC_{50} differences was determined by Type II analysis of variance (ANOVA). ANOVA *p*-values were subjected to Benjamini-Hochberg multiple testing correction, and associations with false discovery rate <20% were considered significant.

Cell line *TP53* missense mutation status. *TP53* missense mutations were retrieved from the DepMap database (version 22Q4). Only cell lines which had at least one missense mutation were selected for further analysis. Cell lines were grouped based on the specific *TP53* residue position which was affected by the missense mutation. Missense mutation positions affected in at least three cell lines were selected for further analysis. Significance of IC_{50} difference was determined as described above.

Correlation analysis 120 reference anti-cancer agents. IC_{50} values for 120 anti-cancer reference agents profiled on 102 of the 115 cell lines were determined in a similar fashion as SJ3149 (Uitdehaag et al., 2016). Pearson correlations were calculated between SJ3149 $^{10}\log IC_{50}$ values and those of the 120 reference agents, to determine the similarity of compound IC_{50} fingerprints.

Correlation analyses gene expression or gene dependency. Cell line RNA sequencing-based basal gene expression values (log2(TPM+1)) and CRISPR dependency scores were retrieved from the DepMap database (version 22Q2 and 22Q4, respectively). SJ3149 or nutlin-3a cell line drug response was related to gene expression or gene dependency by calculating Pearson correlations between the $^{10}\log IC_{50}$ values and either gene expression values or gene dependency scores in the same cell lines.

Protein Expression and Purification: Truncated human CRBN (StrepII-CRBN$^{\Delta 1\text{-}40}$) and human DDB1 (His_6-DDB1$^{\Delta BPB}$)[65] were co-expressed in Trichoplusia ni High-Five insect cells using the BestBac 2.0 baculovirus expression system (Expression Systems). Human full-length CK1α (StrepII-CK1α) was synthesized and cloned into the pFastBac1 vector (Genscript) and expressed in High-Five insect cells using the Bac-to-Bac baculovirus expression system (Invitrogen). StrepII-CRBN$^{\Delta 1\text{-}40}$-His_6-DDB1$^{\Delta BPB}$ cells were resuspended in 50 mM Tris-HCl pH 8.0, 200 mM NaCl, 1 mM TCEP, 10% glycerol, 50 µM Zinc Acetate, and SigmaFast protease cocktail inhibitor (Millipore Sigma). StrepII-CK1α cells were resuspended in 50 mM Tris-HCl pH 8.0, 500 mM NaCl, 0.25 mM TCEP, 1 mM PMSF, 10% glycerol and SigmaFast protease cocktail inhibitor. Both StrepII-CRBN$^{\Delta 1\text{-}40}$-His_6-DDB1$^{\Delta BPB}$ and StrepII-CK1α were lysed by sonication (2s ON, 2s OFF, 3 min) and clarified by centrifugation (136,000g) for 1.5 hours at 4°C and loaded onto StrepTactin Sepharose resin (IBA) equilibrated in 50 mM Tris-HCl pH 8.0, 200 mM NaCl, 0.25 mM TCEP,

and 10% glycerol. Resin was washed and proteins were eluted with equilibration buffer supplemented with 50 mM Biotin. The StrepII fusion tag of CK1α was cleaved using TEV protease (PPF). Both cleaved CK1α and StrepII-CRBN$^{\Delta 1\text{-}40}$-His_6-DDB1$^{\Delta BPB}$ were buffer exchanged and purified by size exclusion chromatography (S200 10/300 Increase) in the presence of 50 mM HEPES pH 7.4, 200 mM NaCl, and 0.25 mM TCEP. Protein fractions were pooled and concentrated to 70 μM (StrepII-CRBN$^{\Delta 1\text{-}40}$-His_6-DDB1$^{\Delta BPB}$) and 80 μM (CK1α) for crystallization experiments.

Crystallization and Data Collection: For crystallization of the StrepII-CRBN$^{\Delta 1\text{-}40}$-His_6-DDB1$^{\Delta BPB}$-SJ3149-CK1α complex, 70 μM StrepII-CRBN$^{\Delta 1\text{-}40}$-His_6-DDB1$^{\Delta BPB}$ was mixed and incubated with 35 μM SJ3149 before the addition of 80 μM CK1α. The mixture was incubated on ice for 1 h and subsequently centrifuged at 20,000g for 30 min at 4°C. 24-well sitting drop crystallization plates (Hampton) were set up by mixing protein 1:1 with reservoir solution containing 70 mM Tris pH 7.0, 140 mM $MgCl_2$ and 10% (w/v) PEG8000 and plates were incubated at room temperature. Crystals appeared after 24 h and continued growing for 14 days via vapor diffusion. Crystals were cryo-protected in reservoir solution supplemented with 20% ethylene glycol and flash-cooled in liquid nitrogen. Diffraction data were collected at SER-CAT (beamline 22-ID) to a resolution of 3.45 Å.

Structure Determination and Model Building: Data collection and refinement statistics are provided in Table SB1. The P1 data was integrated and scaled in XDS, scaling two different datasets from the same crystal using XSCALE.[66] The structure was solved by Molecular Replacement with 5FQD as the search model using Phaser.[67] The asymmetric unit contained two ternary complexes, with ABC and DEF corresponding to DDB1, Cereblon and CK1alpha, respectively. SJ3149 is unambiguously modeled at the cereblon-CK1 alpha interface in the ABC quaternary complex. SJ3149 was not modeled in the DEF complex due to insufficient electron density. Model building and refinement were performed in COOT[68] and Phenix[69], respectively. The ABC complex electron density is of higher quality relative to DEF and is referred to throughout the manuscript.

Figures

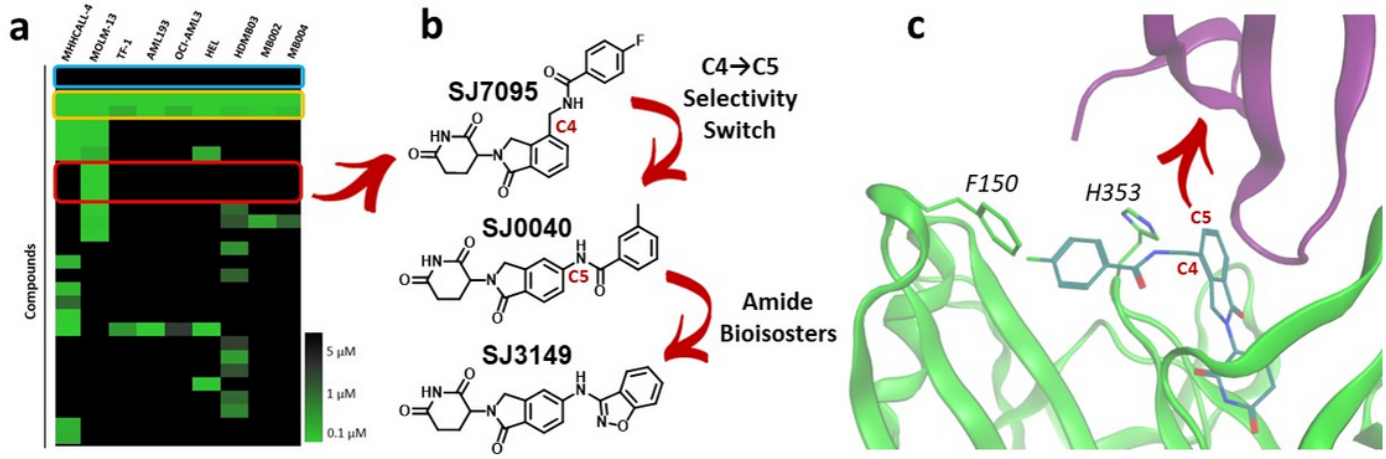

Figure 1

Hit identification and optimization strategy. a. Heatmap of selected screening hits across a panel of acute leukemia (AL) and medulloblastoma (MB) cell lines (cell viability IC_{50} values determined by CTG assays). The blue box highlights lenalidomide and pomalidomide, yellow box highlights known GSPT degraders CC-885 and SJ6986, red box highlights MOLM-13 hits. **b.** Optimization trajectory and chemical structures of the hit and leads. **c.** SJ7095 (shown as cyan sticks) modeled into the lenalidomide+CRBN (green)+CK1a (purple) complex (PDB: 5FQD).[28] The red arrow points to the C5-substitution vector that underlined the optimization strategy.

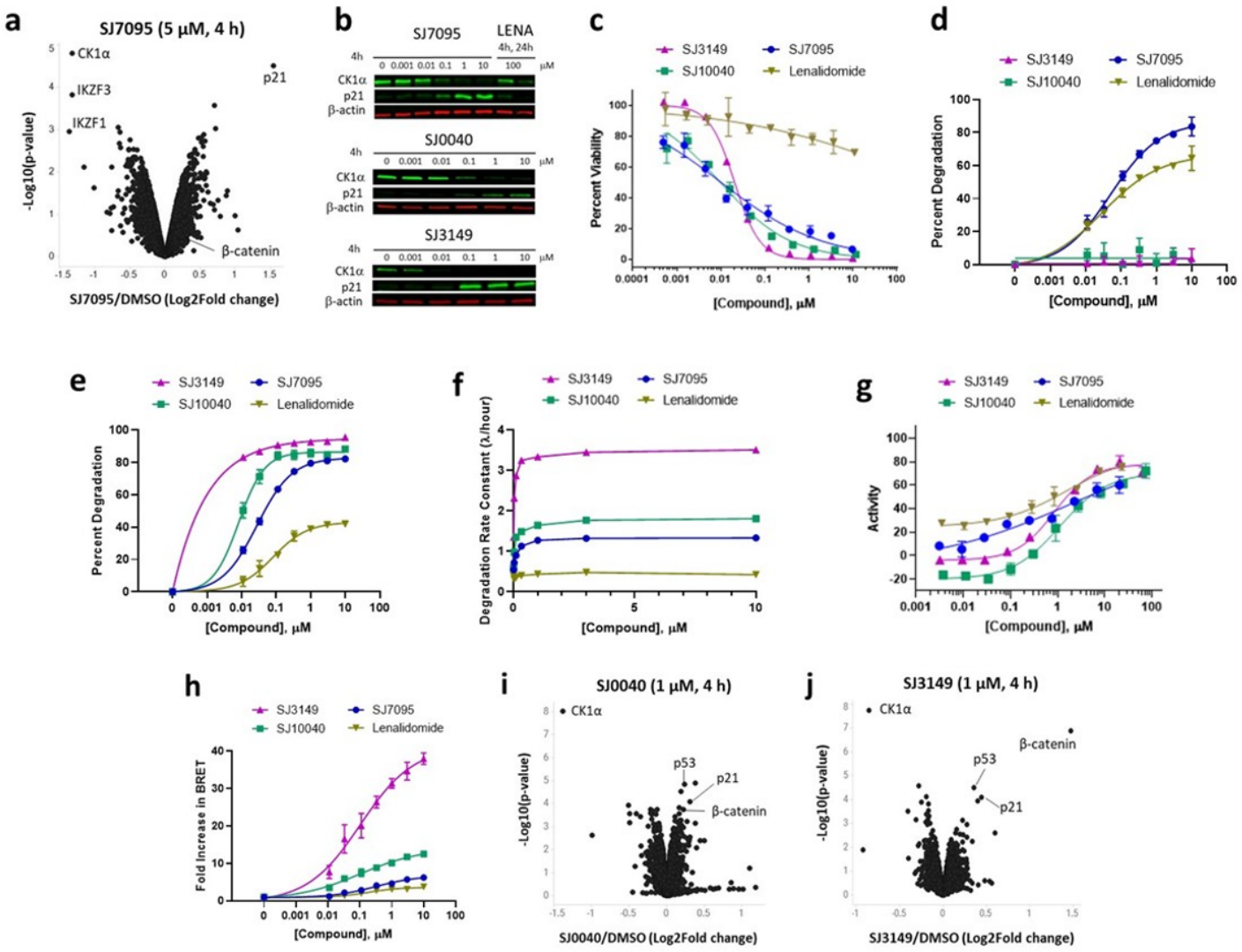

Figure 2

Degradation profiles of hit and leads. Data represents the average of at least 3 independent determinations. Error bars represent standard error of the mean. **a.** TMT-Proteomics in MOLM-13 cells following 4 h treatment with SJ7095 at 5 µM concentration. **b.** CK1α and p21 protein levels in MOLM-13 cells determined by immunoblotting following treatment with increasing concentrations of test compound over 4 hours, and lenalidomide at 100 mM over 4 and 24 hours. The CK1a DC_{50} value was calculated using quantified band intensities from the immunoblotting analysis. **c.** MOLM-13 cells viability measured in the CTG assay after 72 h incubation with rising concentrations of tested compound. **d.** IKZF1 degradation maximum (D_{max}) as determined by IKZF1 HiBiT assay. **e.** CK1a degradation maximum (D_{max}) as determined by CK1a HiBiT assay. **f.** CK1a degradation rate as determined by CK1a HiBiT assay. **g.** Cereblon binding affinity determined in the fluorescence polarization (FP) displacement assay. **h.** Ternary complex formation measured in CK1a-CRBN NanoBRET assay. TMT-Proteomics in MOLM-13 cells following 4 h treatment with 1 µM concentration of: **i.** SJ0040, and **j.** SJ3149.

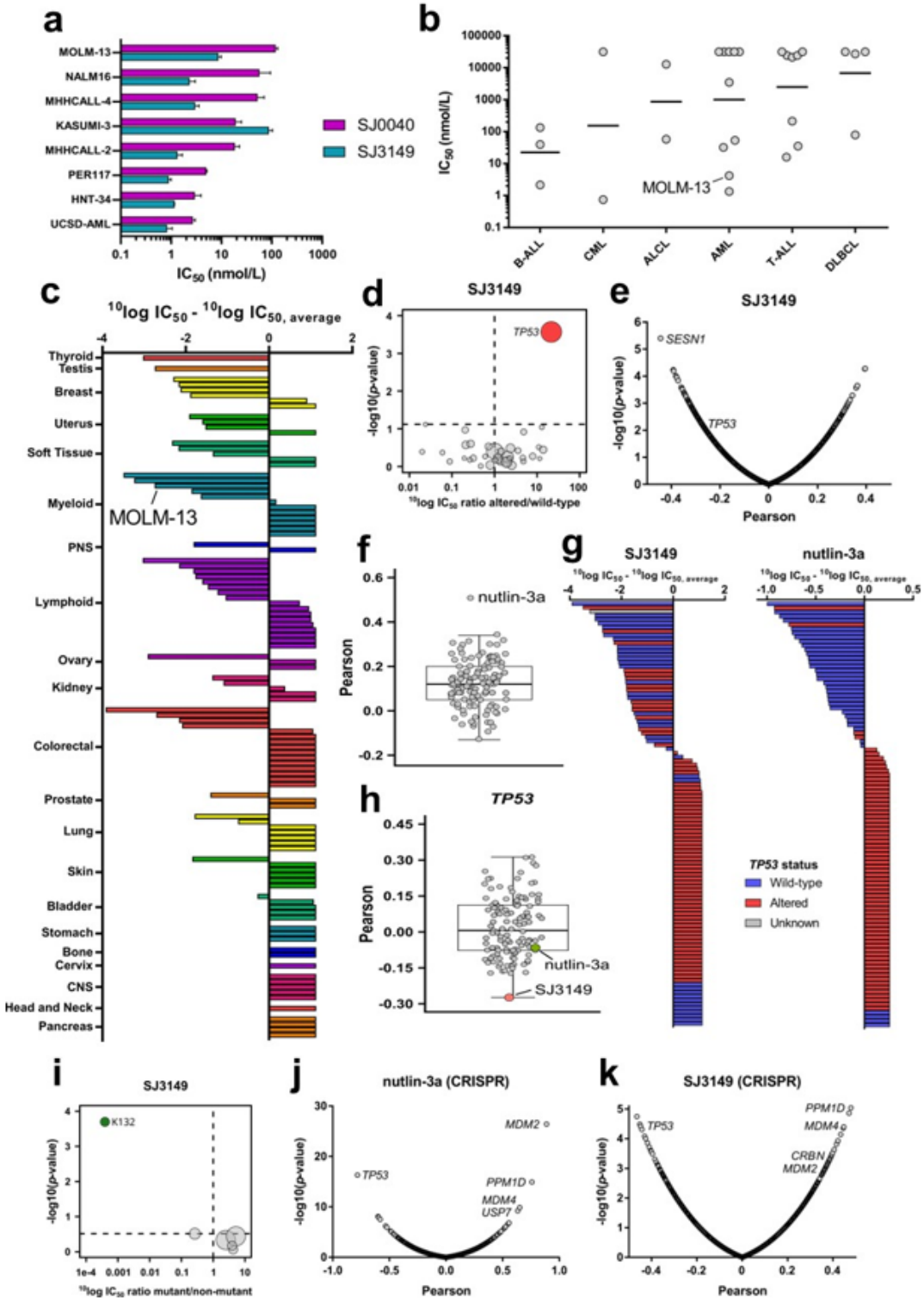

Figure 3

Analysis of SJ3149 activity in a broad range of human cancer cell lines. a. IC_{50} values of SJ0040 and SJ3149 in a panel of AL cell lines. Error bars represent standard error of the mean (n=3). **b.** Scatterplot of the IC_{50} distribution of SJ3149 in hematologic cell lines. Cell lines were grouped based on their disease subtype. Horizontal solid lines indicate the geometric means. **c.** Waterfall plots of cellular responses to SJ3149. Cell lines were grouped and colored based on their tissue of origin. **d.** Volcano plot comparing

compound SJ3149 IC_{50} differences between altered and wild-type cell lines for 38 established cancer genes. The red node indicates significantly higher IC_{50} in the *TP53*-altered cell lines, as determined by ANOVA. **e.** Volcano plot of Pearson correlations between SJ3149 IC_{50} values and basal expression levels of 19,146 genes in 99 cell lines. **f.** Boxplot of Pearson correlations between SJ3149 IC_{50} values and IC_{50} values of 120 anti-cancer agents in 102 cell lines. **g.** Waterfall plots of cellular response to SJ3149 (left) and nutlin-3a (right). Cell lines were colored based on the genomic status of *TP53*. **h.** Boxplot of Pearson correlations between basal expression levels of *TP53*, and IC_{50} values of SJ3149 and the 120 anti-cancer agents. SJ3149 is indicated in red, nutlin-3a in green, and all other compounds in grey. **i.** Volcano plot comparing the compound SJ3149 IC_{50} differences between cell lines harboring *TP53* missense mutations. The green node indicates significantly lower IC_{50} in cell lines harboring a missense mutation on residue K132, as determined by ANOVA. Volcano plot of the Pearson correlations between drug IC_{50} values and CRISPR dependency scores of 17,453 genes in 77 cell lines for **j.** nutlin-3a, and **k.** SJ3149. Correlations are based on 78 cell lines.

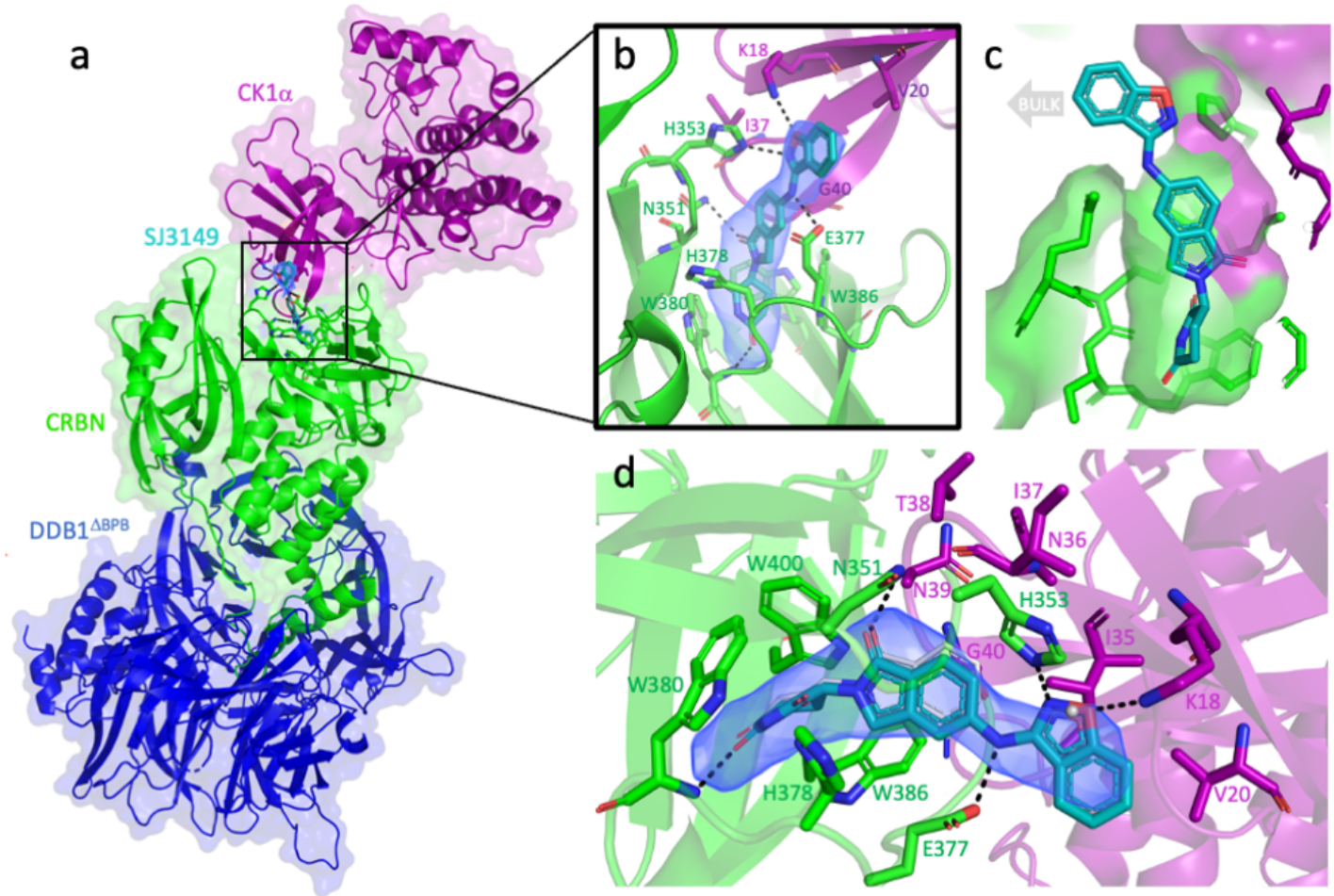

Figure 4

Quaternary complex of CK1α+CRBN$^{\Delta 1\text{-}40}$+DDB1$^{\Delta BPB}$+SJ3149. a. Quaternary complex of CK1α (purple) and CRBN (green) DDB1 (blue) in the presence of molecular glue SJ3149 (shown as cyan sticks). **b.** The magnified region of the binding interface of CK1α and CRBN that accommodates SJ3149 with hydrogen bonds shown as dashed lines. **c.** Surface representation of the SJ3149 binding pocket with the benzisoxazol exposed to bulk solvent and available for chemical modification. **d.** The Fo-Fc electron density map (rendered at 2.5 sigma) of the ligand allows the unambiguous placement of SJ3149 in the binding site with the novel benzisoxasol moiety extending to directly H-bond with K18 of CK1α, and H353 and E377 of CRBN. Overlay of the lenalidomide quaternary complex (5FQD; lenalidomide shown as thin grey sticks) shows similar accommodation of the shared glutarimide moiety and the displacement of a water molecule (grey sphere) that was observed in the lenalidomide-bound complex upon SJ3149 binding.

Supplementary Files

This is a list of supplementary files associated with this preprint. Click to download.

- SIfinal.docx
- EXTENDEDDATA.docx
- ck1arotation.mp4